CONFIDENTIAL

Copy 286
RM L53G28

NACA

RESEARCH MEMORANDUM

A THEORY FOR STABILITY AND BUZZ PULSATION AMPLITUDE IN RAM JETS AND AN EXPERIMENTAL INVESTIGATION INCLUDING SCALE EFFECTS

By Robert L. Trimpi

Langley Aeronautical Laboratory
Langley Field, Va.

CLASSIFIED DOCUMENT

[redacted]

NATIONAL ADVISORY COMMITTEE
FOR AERONAUTICS

WASHINGTON
October 15, 1953

CONFIDENTIAL

Space Administration

Langley Research Center
Hampton, Virginia
23665

Reply to Attn of 139A

JUN 16 1983

TO: Distribution

FROM: 180A/Security Classification Officer

SUBJECT: Authority to Declassify NACA/NASA Documents Dated Prior to January 1, 1960

Effective this date, all material (informal, correspondence) classified by this Center prior to January 1, 1960, is declassified. This action does not include material derivatively classified at the Center upon instructions from other Agencies.

Immediate re-marking is not required; however, until material is re-marked by lining through the classification and annotating with the following statement, it must continue to be protected as if classified:

> "Declassified by authority of LaRC Security Classification Officer (SCO) letter dated June 16, 1983," and the signature of person performing the re-marking.

If re-marking a large amount of material is desirable, but unduly burdensome, custodians may follow the instructions contained in NHB 1640.4, subpart F, section 1203.604, paragraph (h).

This declassification action complements earlier actions by the National Archives and Records Service (NARS) and by the NASA Security Classification Officer (SCO). In Declassification Review Program 807008, NARS declassified the Center's "Research Authorization" files, which contain reports, Research Authorizations, correspondence, photographs, and other documentation. Earlier, in a 1971 letter, the NASA SCO declassified all NACA/NASA formal series documents with the exception of the following reports, which must remain classified:

Document No.	First Author
E-51A30	Nagey
E-53G20	Francisco
E-53G21	Johnson
E-53K18	Spooner
SL-54J21a	Westphal
E-55C16	Fox
E-56H23a	Himmel

JUN 23 1983

If you have any questions concerning this matter, please call Mr. William L. Simkins at extension 3281.

Jess G. Ross
2898

Distribution:
SDL 031

cc:
NASA Scientific and Technical
Information Facility
P.O. Box 8757
BWI Airport, MD 21240

NASA--NIS-5/Security
180A/RIAD
139A/TU&AO
139A/WLSimkins:elf 06/15/83 (3281)
139A/JS 6-15-83

31-01 HEADS OF ORGANIZATIONS
HESS, JANE S.,
MAIL STOP 185 BLDG 1194

NATIONAL ADVISORY COMMITTEE FOR AERONAUTICS

RESEARCH MEMORANDUM

A THEORY FOR STABILITY AND BUZZ PULSATION AMPLITUDE IN RAM JETS AND AN EXPERIMENTAL INVESTIGATION INCLUDING SCALE EFFECTS

By Robert L. Trimpi

SUMMARY

From a theory developed on a quasi-one-dimensional-flow basis, it was found that the stability of the ram jet is dependent upon the instantaneous values of mass flow and total pressure recovery of the supersonic diffuser and immediate neighboring subsonic diffuser. Conditions for stable and unstable flow were presented. The theory developed in the report was in agreement with the experimental data of the reports both of Sterbentz and Evvard and of Ferri and Nucci.

It was shown that the model assumed in the resonator analysis of Sterbentz and Evvard may be considered a rough approximation to the actual phenomena when applied for purposes of obtaining the general trends and orders of magnitude of frequency and amplitude of oscillation providing the wave length of the highest frequency component of the oscillation be much larger than the length of the ram jet. The resonator analysis is not applicable when considering the initial stability of the inlet without combustion and should not be so applied to obtain such stability criteria.

A simple theory for predicting the approximate amplitude of small pressure pulsation in terms of mass-flow decrement from minimum-stable mass flow was developed and found to agree with experiments.

Cold-flow tests at a Mach number of 1.94 of ram-jet models having scale factors of 3.15:1 and Reynolds number ratios of 4.75:1 with several supersonic diffuser configurations showed only small variations in performance between geometrically similar models. The predominant variation in steady-flow performance resulted from the larger boundary layer in the combustion chamber of the low Reynolds number model. The conditions at which buzz originated were nearly the same for the same supersonic diffuser (cowling-position angle) configurations in both large and small diameter models. There was no appreciable variation in stability limits of any of the models when the combustion-chamber

length was increased by a factor of three. The unsteady-flow performance and wave patterns were also similar when considered on a reduced-frequency basis depending on the relative lengths of the model. The negligible effect of Reynolds number on stability of the off-design configurations was not anticipated in view of the importance of boundary layer to stability, and this result should not be construed to be generally applicable.

The velocity profile in the combustion chamber at both Reynolds numbers was appreciably influenced by an angle of attack of $1/2^{\circ}$. The external shock pattern was noticeably affected only for the lower cowling-position angles. The pressure recovery and mass-flow values at the start of buzz were not noticeably affected.

INTRODUCTION

The buzzing, or oscillation, of the shock configuration at the inlet of supersonic diffusers has been the subject of many investigations since 1944 when Oswatitsch (ref. 1) first encountered the phenomenon in axisymmetric inlets with central bodies. Recent research has shown that buzzing is not limited to axisymmetric conical center-body inlets but is also associated with scoop-type inlets (ref. 2) and perforated convergent-divergent diffusers (ref. 3).

The operation of ram jets at off-design conditions due to flight speeds less than the design speed or due to various fuel-air ratios, as well as maneuvering at design speed, results in operation at reduced values of mass flow; in other words, the area of the stream tube swallowed by the inlet is smaller than the cross-sectional area of the inlet. In order to obtain this reduced mass flow there must be a change in the shock pattern of the inlet. In the axisymmetric center-body-type inlet any reduction in mass flow over that accomplished by the deflection of the stream lines across the conical shock can be obtained only as a result of the second or so-called "normal shock," which is usually at or to the rear of the cowling entrance at design Mach number, moving forward to effect mass-flow spillage in the subsonic region existing just behind it. The mass-flow reduction in the various other types of inlet is also mainly dependent on the "normal shock." Buzzing occurs when the flow pattern becomes unstable at the position to which the normal shock is forced to move in order to satisfy the particular mass-flow requirements of the ram jet.

The performance of a diffuser is reduced by instability (ref. 4) and in addition the resulting pressure fluctuations can produce serious combustion and structural problems depending on the oscillation amplitude. Consequently, it is essential for efficient operation that the buzzing be either eliminated, avoided, or its amplitude controlled at a small value.

Various criteria for determining the cause of instability have previously been reported. Reference 5 expounds the effects of a vortex-sheet-induced separation as one cause, whereas reference 6, and others, have shown separation on the central body to be another contributing factor in absence of combustion instability or rough burning. In addition to the aforementioned theories based on fundamental aerodynamic phenomena, a modified Helmholtz resonator concept (ref. 7) has been proposed to predict the onset of instability as a function of the slope of the mean pressure-recovery mass-flow curve.

Reference 8 proposes a stability criterion, based only on the steady flow ahead of the cowling, in which a zero slope of the cowling static pressure versus mass-flow curve predicts the start of buzz. Experimental results, however, have shown that the flow to the rear of the inlet lip can influence stability.

The mechanism for the continuation of the cold-flow-buzzing cycle, once it has been initiated, was investigated in reference 6 and the various traveling waves moving up and down the ram jet were theoretically computed on a quasi-one-dimensional basis and found to agree closely with experimental results. However, an experimental value of the strength of the initial wave had to be used as a starting point for the computations.

Since predictions of the buzzing phenomena by any of the methods described have not been infallible, the only recourse in determining the behavior of a particular ram jet has been to actually test the configuration. The testing of full-scale units is both difficult and costly so that the obvious solution is the testing of small-scale models, providing the model behavior can be properly correlated with the actual ram jet for both steady and unsteady flow.

A possible method for predicting the amplitude of the pressure oscillations, based on a further modification of the Helmholtz resonator concept previously mentioned, was proposed in reference 9. Again an experimental point was used to get a basis from which to make further involved computations. Furthermore, the procedure required to obtain the amplitude by this method is quite involved and lengthy so that it would be advantageous to have a simple short method for amplitude prediction.

A theoretical and experimental investigation was conducted at Langley to gain further information regarding the cold flow stability limits for buzzing and regarding model scale effects in steady and time-dependent flow. In addition, a simple approximate theory for predicting pulsation amplitude was derived on a linearized one-dimensional accoustical basis.

SYMBOLS

$a,(\delta a)$	local speed of sound, (perturbation to local speed of sound)
f,g	functional solutions to wave equation
m	mass flow through model
m_b	mass flow through model at start of buzz
m_o	mass flow at infinity through a stream tube of diameter equal to cowling-lip diameter
n	integer denoting number of wave traversals in each oscillation cycle (equivalent to quotient of oscillation wavelength divided by twice ram-jet length)
$p,(\Delta p,\delta p)$	pressure, (pressure perturbation)
r	radius of model
r_o	radius of outer rake tube
t	time
w	turbulence velocity
x	axial distance measured from cowling lip
C_1,C_2,C_3,C_4	constants defined in equations
D	nominal (maximum internal) diameter of models
F,G	functional solutions to wave equation
L	length of model
M	Mach number
R	gas constant
R_o	maximum internal radius of model
$U(\Delta U,\delta U)$	fluid speed in ram jet, (perturbation to fluid speed)

V	fluid speed in free stream
V_{max}	maximum fluid speed if fluid is expanded to zero pressure
α	angle of attack, deg
γ	ratio of specific heats, assumed equal to 1.40
ξ	axial coordinate in moving wave system
$\rho,(\Delta\rho,\delta\rho)$	density, (perturbation density)
μ	viscosity
τ	period of oscillation
ω	frequency of oscillation
$\phi,(\delta\phi)$	velocity potential, (perturbation potential)

Subscripts indicate following states unless otherwise noted above:

b	start of buzz
o	local stagnation conditions
∞	free stream

THEORY FOR APPROXIMATE PRESSURE AMPLITUDE OF BUZZ

A low-amplitude buzzing, while not beneficial to the performance of a propulsion unit, might under certain circumstances (such as a particular off-design operation encountered only for short-time periods) be less undesirable than the performance penalty required to avoid buzzing completely. It would then be advantageous to be able to predict the amplitude of buzzing as a function of mass flow. Reference 9 presents one method, based on resonator principles, which is not only lengthy and tedious but also yields a constant amplitude throughout the combustion chamber in contrast to experimental data which show varying amplitude. Consequently a simple linear theory has been derived to permit facile computations of the relation of pressure amplitude at various positions in the ram jet to mass flow.

A linearized equation of motion for small disturbances superimposed on a one-dimensional isentropic steady flow may be obtained by neglecting products of perturbations, of the derivatives of perturbations, of the

perturbations and derivatives of perturbations, etc., in respect to the first power of said perturbations. Let the steady flow be defined by the parameters U, p, ρ, and a. Then the unsteady flow is defined by $U + \delta u(x,t)$, $p + \delta p(x,t)$, $\rho + \delta\rho(x,t)$, and $a + \delta a(x,t)$. For the above conditions and restrictions the equations of continuity and momentum become (when subscripts denote partial differentiation)

$$\delta\rho_t + U\,\delta\rho_x + \rho\,\delta U_x = 0 \tag{1}$$

$$\delta U_t + U\,\delta U_x = -\frac{1}{\rho}\frac{dp}{d\rho}\,\delta\rho_x \tag{2}$$

Differentiating equation (1) with respect to x and equation (2) with respect to time gives

$$\delta\rho_{xt} + U\,\delta\rho_{xx} + \rho\,\delta U_{xx} = 0 \tag{3}$$

$$\delta U_{tt} + U\,\delta U_{xt} = -\frac{1}{\rho}\frac{dp}{d\rho}\,\delta\rho_{xt} \tag{4}$$

Combining equations (3) and (4) results in the following equation:

$$\frac{1}{\rho}\frac{dp}{d\rho}\left[U\,\delta\rho_{xx} + \rho\,\delta U_{xx}\right] = \delta U_{tt} + U\,\delta U_{xt} \tag{5}$$

Differentiating equation (2) with respect to x leads to

$$\delta U_{xt} + U\,\delta U_{xx} = -\frac{1}{\rho}\frac{dp}{d\rho}\,\delta\rho_{xx} \tag{6}$$

Substituting equation (6) in equation (5) and rearranging, using $a^2 \equiv \frac{dp}{d\rho}$, yields the following differential equations:

$$-U\,\delta U_{xt} - U^2\,\delta U_{xx} + \frac{dp}{d\rho}\,\delta U_{xx} = \delta U_{tt} + U\,\delta U_{xt} \tag{7}$$

$$\delta U_{tt} = \left(a^2 - U^2\right)\delta U_{xx} - 2U\,\delta U_{xt} \tag{8}$$

[redacted]

It may be verified by substitution that solutions of equation (8) are to be found in the form

$$\delta U = f\left[x - (U + a)t\right] + g\left[x - (U - a)t\right] \tag{9}$$

The first term represents a wave moving with a velocity of $U + a$ and the second a wave traveling with a velocity $U - a$.

These solutions are to be expected since if a potential $\phi = Ux + \delta\phi$ exists, where $\delta U = \delta\phi_x$, equation (8) becomes, after partial integration with respect to x,

$$\delta\phi_{tt} = \left(a^2 - U^2\right)\delta\phi_{xx} - 2U\,\delta\phi_{xt} \tag{10}$$

Equation (10) could also have been obtained from the simple wave equation, $\phi_{\xi\xi} = \frac{1}{a^2}\phi_{tt}$, for a disturbance in a fluid at rest by a transformation of coordinates to account for the fluid motion. Solutions of the wave equation are known to be of the form $\delta U = f(\xi - at) + g(\xi + at)$, and replacing ξ by $x - Ut$ yields equations (9) and (10).

Substitution of equation (9) in equation (2) and integrating with respect to x yields the perturbation density:

$$\frac{\delta\rho}{\rho} = \frac{f\left[x - (U + a)t\right] - g\left[x - (U - a)t\right]}{a} \tag{11}$$

Applying the isentropic relationships to determine the other perturbations yields

$$\frac{\delta p}{p} = \gamma\frac{\delta\rho}{\rho} = \gamma\frac{f\left[x - (U + a)t\right] - g\left[x - (U - a)t\right]}{a} \tag{12}$$

$$\frac{\delta a}{a} = \frac{\gamma - 1}{2}\frac{\delta\rho}{\rho} = \frac{\gamma - 1}{2}\frac{f\left[x - (U + a)t\right] - g\left[x - (U - a)t\right]}{a} \tag{13}$$

Equations (9), (11), (12), and (13) are the general equations applicable to a one-dimensional steady flow with unsteady perturbations.

If these equations are to be applied to the ram jet, considered as a constant area duct with a constriction at the exit, the proper boundary condition at the exit must be considered. In reference 6 it was shown that consistent with the assumption of a choked nozzle was the assumption of constant Mach number at the end of the duct for a given nozzle area. Now, for $M = \text{Constant} = \frac{U}{a} = \frac{U + \delta U}{a + \delta a}$ at the exit,

$$M = \frac{U}{a} = \frac{U + \delta U}{a + \delta a} = \frac{U}{a}\left[1 + \frac{\delta U}{U} - \frac{\delta a}{a} + \cdots\right] \tag{14}$$

Therefore,

$$\frac{\delta U}{U} = \frac{\delta a}{a}$$

$$\frac{f + g}{U} = \frac{\gamma - 1}{2}\left(\frac{f - g}{a}\right) \qquad (\text{at } x = L)$$

$$\frac{f(L,t)}{g(L,t)} = + \frac{\frac{\gamma - 1}{2} M + 1}{\frac{\gamma - 1}{2} M - 1} \tag{15}$$

Equation (15) relating the strengths of the downstream and upstream waves at the exit is similar to equation (6) of reference 6 which gives the value of these waves for the exact characteristic solution.

Closed solutions satisfying equations (9) and (15) may be found in harmonic form. Since the sine wave form often occurs in buzzing, a simple expression for that type of wave is shown in the following equation, where C_1 is as yet an undetermined constant dependent on the amplitude and ω is the frequency of the oscillation:

$$\frac{\delta U}{C_1} = \frac{\frac{\gamma - 1}{2} M + 1}{\frac{\gamma - 1}{2} M - 1} \sin\left\{\frac{2\pi\omega}{(1 - M^2)a}\left[(M - 1)x + (1 - M^2)at + L\right]\right\} +$$

$$\sin\left\{\frac{2\pi\omega}{(1 - M^2)a}\left[(M + 1)x + (1 - M^2)at - L\right]\right\} \tag{16}$$

Note that the boundary condition for $x/L = 1$, equation (15), is identically satisfied for all times. Furthermore, if each cycle requires n waves to traverse the ram jet in both directions during a period τ, then

$$\frac{1}{\omega} = \tau = n\left(\frac{L}{U + a} + \frac{L}{a - U}\right) = \frac{2nL}{a\left(1 - M^2\right)}$$

and

$$\frac{\delta U}{C_1} = \frac{\frac{\gamma - 1}{2} M + 1}{\frac{\gamma - 1}{2} M - 1} \sin\left[(M - 1)\frac{\pi x}{nL} + \frac{\pi}{n} + 2\pi\frac{t}{\tau}\right] + \sin\left[(M + 1)\frac{\pi x}{nL} - \frac{\pi}{n} + \frac{2\pi t}{\tau}\right] \tag{17}$$

From the above equation, where the first term on the right-hand side represents f and the second g, and equations (11) and (12), one finds the relationship between the perturbation amplitudes of pressure and density:

$$\frac{\delta\rho}{\rho}\frac{a}{C_1} = \frac{\delta p}{p}\frac{a}{\gamma C_1} = \frac{\frac{\gamma - 1}{2} M + 1}{\frac{\gamma - 1}{2} M - 1} \sin\left[(M - 1)\frac{\pi x}{nL} + \frac{\pi}{n} + 2\pi\frac{t}{\tau}\right] - \sin\left[(M + 1)\frac{\pi x}{nL} - \frac{\pi}{n} + 2\pi\frac{t}{\tau}\right] \tag{18}$$

Corresponding equations, though not in such simple form, may be found for any desired shape of a pressure-time curve by approximating the curve by straight-line segments for which the equations are linear in time.

The problem of determining the pressure perturbation at any time and at any value of x is then reduced to a determination of the constant C_1. An approximation to this value for small amplitudes may be obtained in the following manner where perturbations are applied to the average mass flow which varies slightly from the incipient mass flow

at start of buzz. Time-averaged quantities are denoted by a bar and the following identities employed:

$$\left.\begin{aligned} \bar{\rho} &\equiv \rho_b - \Delta\rho \\ \bar{U} &\equiv U_b - \Delta U \\ \bar{p} &\equiv p_b - \Delta p \end{aligned}\right\} \tag{19}$$

$$\bar{m} = \text{Average mass flow} = \bar{\rho}\,\bar{U} \tag{20}$$

$$\frac{\bar{m}}{m_b} = \frac{\bar{m}}{\rho_b U_b} = 1 - \frac{\Delta\rho}{\rho_b} - \frac{\Delta U}{U_b} \tag{21}$$

$$\frac{\bar{m}}{m_b} = 1 - \frac{\Delta p}{\gamma p_b} - \frac{\Delta U}{U_b} \tag{21a}$$

The assumption is then introduced that at the midpoint of the ram jet the maximum variations (amplitude) in pressure and velocity are equal to the difference between the incipient values and the average values, that is, at $x/L = 1/2$

$$\left.\begin{aligned} |\delta p|_{\text{max positive}} &= \Delta p \\ |\delta u|_{\text{max positive}} &= \Delta u \end{aligned}\right\} \tag{22}$$

Some justification for the pressure approximation may be found in figures 2 and 8 of reference 10 and figure 1 of this report (gage 3 at $x/L = 0.6$) which show the peak pressure to be approximately the incipient value for buzzing near the midpoint of the ram jet for small amplitudes in cold flow. When combustion is present, references 4 and 8 show that the peak pressures are slightly below the cold flow incipient value until a buzz giving optimum average static pressure (highest manometer pressure noted during buzzing) is reached at which point the average pressure is equal to the optimum static pressure in cold flow (incipient pressure) less the amplitude of pressure pulsation.

No data are available for substantiation of the corresponding velocity assumption. However, it would seem logical to apply similar boundary conditions at the same point. Also, since at the midpoint of the ram jet the values of the velocity and pressure perturbation amplitude are between the maximum and minimum values existing at the extremities of the ducting; this midpoint would further appear to be the desirable place to evaluate amplitudes.

This assumption relating amplitudes to average and incipient values will apply only for small values of the oscillation and even then it is only an approximation in some cases. However, since it will give an easy method of determining the approximate pressure amplitudes, its use is justifiable providing the limits imposed are considered in analyzing results obtained. The mass-flow-weighted values of U_b and a_b should be used in the computations where boundary-layer effects cause a nonuniformity in parameters across the channel.

Thus, the following approximation is determined:

$$\frac{\bar{m}}{m_b} = 1 - \frac{1}{\gamma}\left|\frac{\delta p}{p}\right|_{\substack{\text{max positive} \\ x/L = 1/2}} - \left|\frac{\delta U}{U}\right|_{\substack{\text{max positive} \\ x/L = 1/2}} \tag{23}$$

$$\frac{\bar{m}}{m_b} = 1 - \left|\frac{f - g}{a_b}\right|_{\substack{\text{max positive} \\ x/L = 1/2}} - \left|\frac{f + g}{U_b}\right|_{\substack{\text{max positive} \\ x/L = 1/2}} \tag{24}$$

In general, if f and g are replaced by C_1F and C_1G where F and G are representative only of the form of the waves of unit amplitude, then equations (9), (12), and (24) become:

$$\delta U = C_1\left[F + G\right] \tag{25}$$

$$\frac{\delta p}{p} = \gamma C_1\left[\frac{F - G}{a}\right] \tag{26}$$

$$1 - \frac{\bar{m}}{m_b} = \frac{C_1}{a_b}\left|F - G\right|_{\substack{\text{max positive} \\ x/L = 1/2}} + \frac{C_1}{a_b}\frac{1}{M_b}\left|F + G\right|_{\substack{\text{max positive} \\ x/L = 1/2}} \tag{27}$$

$$\frac{C_1}{a} = \frac{\left(1 - \frac{\bar{m}}{m_b}\right)}{\left|F - G\right|_{\substack{\text{max positive} \\ x/L = 1/2}} + \frac{1}{M_b}\left|F + G\right|_{\substack{\text{max positive} \\ x/L = 1/2}}} \tag{27a}$$

Equations (26) and (27a) permit the determination of the pressure-time variation for any given value of x/L, M_b, and $\frac{\bar{m}}{m_b}$ for a particular form F and G. In addition, an expression for the total amplitude for any given value of x/L and $\bar{m}/m_b$ may be obtained by maximizing equation (26):

$$\text{Total amplitude}\left(\frac{x}{L}, \frac{\bar{m}}{m_b}\right) = \frac{p_{max} - p_{min}}{p_b}$$

$$= \gamma\left(1 - \frac{\bar{m}}{m_b}\right)\frac{\left|F - G\right|_{\substack{\text{max positive} \\ \text{at } x/L}} - \left|F - G\right|_{\substack{\text{max negative} \\ \text{at } x/L}}}{\left|F - G\right|_{\substack{\text{max positive} \\ x/L = 1/2}} + \frac{1}{M_b}\left|F + G\right|_{\substack{\text{max positive} \\ x/L = 1/2}}} \tag{28}$$

In particular for the sine wave oscillation previously mentioned, the closed form of the equation for total amplitude of pressure pulsation becomes

$$\frac{p_{max} - p_{min}}{p_b} = 2\frac{\Delta p}{p_b}$$

$$= 2\gamma\left(1 - \frac{\bar{m}}{m_b}\right)\left\{\left|\frac{\frac{\gamma-1}{2}M_b + 1}{\frac{\gamma-1}{2}M_b - 1}\right| \sin\left[\left(M_b - 1\right)\frac{\pi x}{nL} + \frac{\pi}{n} + 2\pi\frac{t}{\tau}\right] - \right.$$

$$\left.\sin\left[\left(M_b + 1\right)\frac{\pi x}{nL} - \frac{\pi}{n} + 2\pi\frac{t}{\tau}\right]\right|_{max}\Bigg\}\left\{\left|\frac{\frac{\gamma-1}{2}M_b + 1}{\frac{\gamma-1}{2}M_b - 1}\right| \sin\left[\left(M_b - 1\right)\frac{\pi}{2n} + \right.\right.$$

$$\left.\frac{\pi}{n} + 2\pi\frac{t}{\tau}\right] - \sin\left[\left(M_b + 1\right)\frac{\pi}{2n} - \frac{\pi}{n} + 2\pi\frac{t}{\tau}\right]\Bigg|_{max} + \frac{1}{M_b}\left|\frac{\frac{\gamma-1}{2}M_b + 1}{\frac{\gamma-1}{2}M_b - 1}\right| \sin\left[\left(M_b - \right.\right.$$

$$\left.\left.1\right)\frac{\pi}{2n} + \frac{\pi}{n} + 2\pi\frac{t}{\tau}\right] + \sin\left[\left(M_b + 1\right)\frac{\pi}{2n} - \frac{\pi}{n} + 2\pi\frac{t}{\tau}\right]\Bigg|_{max}\Bigg\}^{-1} . \qquad (29)$$

The maximizing values of $2\pi\frac{t}{\tau}$ for equation (29) are expressed as follows where the upper signs apply to the first brace and first term in the second brace and the lower signs apply to the second term in the second brace:

$$\tan\frac{2\pi t}{\tau} = \frac{\frac{\gamma-1}{2}M_b + 1}{\frac{\gamma-1}{2}M_b - 1}\cos\left[\left(M_b - 1\right)\frac{\pi}{n}\frac{x}{L} + \frac{\pi}{n}\right] \mp \cos\left[\left(M_b + 1\right)\frac{\pi x}{nL} - \frac{\pi}{n}\right] \qquad (30)$$

$$\frac{\frac{\gamma-1}{2}M_b + 1}{\frac{\gamma-1}{2}M_b - 1}\sin\left[\left(M_b - 1\right)\frac{\pi x}{nL} + \frac{\pi}{n}\right] \mp \sin\left[\left(M_b + 1\right)\frac{\pi x}{nL} - \frac{\pi}{n}\right]$$

The determination of the constant C_1 and the amplitudes is slightly more lengthy for waves not expressed in simple closed form (for any time and x/L) such as triangular pulses, etc. In these cases it may be necessary to plot the curves of $\frac{\delta u}{C_1}$ and $\frac{a}{\gamma C_1}\frac{\delta p}{p}$ against time at $x/L = 1/2$ and at any other desired values of x/L to determine the value of the constant C_1 and the maximum value of the term $\frac{a}{\gamma C_1}\frac{\delta p}{p}$. However, computations have shown that the maximized values of the sum and difference of F and G for the same wave forms vary only slightly with M_b if $M_b \ll 1$. Consequently, if the amplitude is to be determined for several adjacent values of M_b the values of $|F \pm G|_{max}$ need be computed for only one value of M_b. Then the total amplitude can be obtained from equation (28) employing these same values of $|F \pm G|_{max}$ but varying M_b in the denominator.

For a given frequency and wave form the theory predicts: (1) a linear increase in pressure amplitude with decrease in mass flow from the incipient value; (2) as n increases with resultant lower frequency for a given mass flow, the amplitude will increase; and (3) higher values of M_b result in larger amplitudes at the same value of n and mass-flow reduction.

APPARATUS

Tests of two different diameter models were conducted in one of the blow-down jets of the Langley Gas Dynamics Branch which uses low humidity air from large pressure tanks. The models were tested at a Mach number of 1.94 ± 0.02 in a jet 5 inches high and 6 inches wide. The test Reynolds number based on cowling-inlet-diameter was 5.7×10^6 for the larger model. The majority of the testing for the small model was done at a Reynolds number of 1.2×10^6. The test-section side walls extended past the end of the nozzle blocks so that the region in which the inlet was located was open to the atmosphere on top and bottom while bounded laterally by the tunnel side walls. The test-section pressure was adjusted to approximately atmospheric pressure for tests of the large model to minimize disturbances near the cowling which was located forward of the Mach lines originating at the ends of the nozzle block. For the small model the pressure was generally below atmospheric in order to lower the Reynolds number further but the flow near the cowling was undisturbed since the shocks from the end of the nozzle intersected the model well aft of the cowling.

In the absence of the models the turbulence level for pressure in the test section was measured by a sting-mounted inductance gage and found to be negligible for the lower test pressures used for the small model. However, the pressure fluctuations reached an amplitude of about 1.6 percent of the test-section pressure for the higher pressure runs.

Owing to misalinement of the model in the tunnel, tests of the large model were made at a positive angle of attack of 1/2°. Consequently, the majority of the small model tests were conducted at this angle of attack, and, in addition, a few pertinent runs were made at angles of attack of 0° and -1/2°.

Two intersecting piano wires were affixed to the outside of the tunnel windows to provide reference lines. The horizontal wire was alined nearly parallel to the center line flow whereas the vertical wire formed an angle of approximately 89° 45' with the horizontal wire in the upper left quadrant.

The models which were constructed to be as geometrically similar as possible are shown schematically in figure 2 where dimensions are presented in terms of nominal combustion-chamber diameters. The diameter for the large model was 4.026 inches (the internal dimensions of 4-inch standard pipe) and for the small model was 1.278 inches, (internal dimension of $1\frac{1}{4}$-inch extra-strong pipe), which gives a scale factor of 3.15 for the two models.

The models will be denoted by three numbers. The first number gives the nominal diameter, the second the length-diameter ratio, and the third the cowling-position parameter (angle between ray from apex of cone to cowling lip and axis of ram jet). Thus, model 4.026 - 14.91 - 44.2° would have a nominal diameter of 4.026 inches, a length-diameter ratio of 14.91, and a cowling-position angle of 44.2°. Omission of any of the numbers will cause no ambiguity since the diameters are 4.026 and 1.278, the length ratios 14.91 and 29.82, and cowling angles are between 40° and 48°. The models are closely similar in over-all internal shape and in external shape in the region rearward as far as 3 diameters from the inlet. In order to use the same plug valve and exhaust system, a transition section was used at the rear of the small model (see fig. 2).

The removable center body was supported by three faired struts 120° apart and provision was made for varying the center-body position in an axial direction by the insertion of spacers between the center body and its strut support. The spacers required to give cowling-position angles of 48.1°, 44.2°, and 40.1° with tolerances of ±0.05° were determined by micrometer measurements. The critical shock angle for a 25° cone at a Mach number of 1.94 is 43° 30'. The ordinates, obtained by micrometer

and surface table measurements, of the cowlings and center bodies are given in table I. The large center body had a conical half-angle of 25.1° and the small body, a half-angle of 25.2°. Fabrication limitations of the small model, rather than aerodynamic considerations, dictated the external cowling design and required an external lip angle of the cowling surface greater than the detachment angle for a Mach number of 1.94. The internal surface at the lip was chosen to be approximately parallel to the flow after the conical shock. Furthermore, the cowlings were not sharp-edged but had flats perpendicular to the model axis of about 0.01 inch and 0.001 inch, respectively, for the large and small models. The variation of area normal to the internal flow with axial distance for cowling-lip angle of 44.2° is shown in figure 3. The small model had a very slight amount of internal contraction just inside the cowling due to an 0.003-inch error in boring out the cowling in the first 0.1 inch of the model. The included conical angle of the internal cowling is 3.75° rearward of $\frac{x}{D} = 0.5$. The central body has a 1.2° included angle after the shoulder. The blockage of the support struts is only about 7 percent of the local cross-sectional area.

The plug valve was operated by a Lear model 440 actuator and the position of the valve was recorded electrically by means of a system employing an NACA control-position transmitter, model 46C (slide-wire resistance), linked to the valve rod.

A nine-tube total-pressure rake with tubes alined in a vertical plane and positioned radially as shown in table II was employed in conjunction with a mercury-differential manometer to determine total-pressure profiles. The three equally spaced support struts were positioned such that the top strut was vertical. Hence, the upper tubes of the rake were in a strut wake, while the lower tubes were unobstructed. Two static orifices located at the rake station were independently connected to the manometer and also to bourdon pressure gages. Pressure in the settling chamber of the nozzle was measured by both bourdon and inductance gages while the pressure in the reference pressure tank of the induction gages was measured by a bourdon gage.

Four 15-pound-per-square-inch NACA miniature electrical pressure gages were flush mounted with the diffuser wall at the axial stations shown in figure 2. These gages were referenced to an air bottle to allow operation at high pressures. A fifth inductance gage was mounted in the settling chamber to compensate for the time lag which might be induced by the long tubing from the settling chamber to the bourdon gage on the manometer board. In addition, a calibrated thermocouple was inserted into the settling chamber.

A General Electric BH-6 mercury-arc lamp was used as the light source for instantaneous and high-speed motion-picture shadowgraphs.

Motion pictures of the shadowgraph image appearing on a ground-glass screen were taken with a Wollensak Optical Company Fastex camera running approximately 350 to 900 frames per second. Signals from the pressure gages were amplified by a Consolidated type 1-113 amplifier and then recorded on sensitized paper in a Consolidated type 5-114 recorder employing galvanometer elements. The frequency response of this system was flat from 2 to 300 cycles per second. In order to correlate movie film with the pressure records, a timing light was attached to one edge of the shadowgraph glass screen and the circuit energizing this light connected in parallel with one of the recording galvanometers so that every time the light flashed, a "blip" appeared on the pressure record. In order to reduce the labor of correlation, an interrupter was placed in the light circuit to stop the flow of current for a noticeable period four or five times a second, and hence provide blank spaces on the film and pressure record which could be easily counted.

The camera photographing the manometer board could be operated either manually or electronically. In the latter mode of operation a pressure pulse in the ram jet caused the camera solenoid to trip and concurrently put a marker on the pressure record.

TEST PROCEDURE

Tests of the various configurations were made in the following manner: After "no-flow" pressure and thermocouple zero traces had been recorded, the plug valve was retracted so that the mass flow through the model would be limited only by the supersonic diffuser configuration. Then, the tunnel was started and brought up to operating conditions. The valve was closed to a position below that which caused instability and a manometer picture and a short pressure record taken. After resetting the manometer camera, the Fastex camera and pressure recorder were then started and the valve closed as slowly as possible until buzz began. The valve was then varied further depending upon the type of run desired. A no-flow pressure trace was made after each run when possible.

Other runs were made to determine steady or, if buzzing, quasi-steady average values. In these cases the manometer and pressure records were taken at various fixed valve positions.

The differential inductance gages and valve-position indicator were calibrated daily. Both the larger and small models were tested at length-diameter ratios of 14.91 and 29.82 for each of the cowling-position parameters of 40.1°, 44.2°, and 48.1°. In addition, the small model was run with no central body in order to get a steady-flow calibration for the effective sonic area of the valve at various positions down to mass flows

approaching zero. Such a series of runs was not made for the large model because of danger of choking the tunnel and in addition because it was felt that with a strong shock far ahead of the inlet that the model would not be free from wall effects.

METHOD OF DATA REDUCTION AND COMPUTATION

The nondimensional mass flow $\frac{\rho U}{\rho_{o_\infty} V_{max}}$ at any rake radius was computed (for steady flow or low amplitude buzzing) from the tank pressure and the local total pressure and static pressure with the assumption that the static pressure was constant across the rake survey plane and stagnation temperature was equal to that in the tank. The local mass flows were then integrated to yield the mass flow in the cross-sectional area bounded by the outer rake tubes. An incremental correction was applied to this mass flow to account for the additional mass flow between the outer rake tube and the wall. In order to determine the constant to be used for adjusting mass flow for the large model, the integrated mass flow was averaged over several runs for configurations 4.026 - 29.82 - 48.1° where a smooth symmetric velocity profile existed at the rake station, and where the mass flow was known since both shocks were swallowed. The average of the local mass flows at the outer rake stations was also determined for these runs. The incremental constant for the large models was then determined as follows:

$$\text{Incremental const.} = \frac{\left(\begin{matrix}\text{Mass flow} \\ \text{for 100\% capture area}\end{matrix}\right) - \left(\begin{matrix}\text{Av. integrated} \\ \text{mass flow}\end{matrix}\right)}{\text{Average local mass flow at outer rake}}$$

The adjusting factor to be applied to each of the integrated-mass-flow curves for the large model was then equal to the product of the incremental constant times the local mass flow value at the outer rake locations, that is:

$$\left(\begin{matrix}\text{Total} \\ \text{mass flow}\end{matrix}\right) = \left(\begin{matrix}\text{Integrated} \\ \text{mass flow}\end{matrix}\right) + \left(\begin{matrix}\text{Incremental} \\ \text{const.}\end{matrix}\right) \times \left(\begin{matrix}\text{Outer rake mass} \\ \text{flow for each run}\end{matrix}\right)$$

The product of the nondimensional local mass flow times pressure recovery $\left(\frac{\rho U p_o}{\rho_{o_\infty} V_{max} p_{o_\infty}}\right)$ was integrated similarly using the correction constant obtained for the mass flow. Assuming the constant to be the same for both pressure recovery and mass flow introduces an error of about 0.1 percent in pressure recovery. The weighted average pressure

recovery was determined as the quotient of the total area under the $\frac{\rho U p_o}{\rho_{o_\infty} V_{max} p_{o_\infty}}$ curve divided by the total area under the $\frac{\rho U}{\rho_{o_\infty} V_{max}}$ curve.

A similar constant was obtained for use in the small model computations by using the average values obtained from swallowed shock runs of configuration 1.278 - 29.82 - 48.1°.

The effective sonic area of the plug valve as it approached the fully closed position was computed for the small model from runs made with the central body removed, a configuration which did not buzz at any mass-flow value. A calibration curve of sonic area against valve position was thus obtained for low-mass flow. This curve in conjunction with the average value of pressure recovery was used to determine the mass flow for the larger amplitude buzz of the small model. The static-pressure—total-pressure method used for steady-flow small-amplitude buzzing become inaccurate in this region since standing waves in the manometer tubing (see ref. 11) gave erroneous pressure readings which, even if small, have a large effect when the difference between static and total pressure becomes small also. This error in pressure would have only a small effect on mass flow computed on a sonic area and total-pressure basis.

The data plotted in figures 4 to 12 were obtained in the manner described above. An examination of figure 4 shows the computed total mass-flow ratios for the high L/D models with swallowed shock to vary only ±1.0 percent from the 100-percent capture mass-flow ratio.

Typical steady-state mass-flow and Mach number profiles for the 29.83 - 48.1° configurations are presented in figures 13 and 14, respectively. Since the Mach number is so small these curves are also close approximations to the velocity profile. Because both the normal and conical shock are inside the cowling, the mass flow is known and the portion of the curve between the outer rake and the wall was assumed to be approximately the cubic equation:

$$\frac{\rho U(r)}{\rho U(r_o)} = C_2\left(1 - \frac{r}{R}\right) + C_3\left(1 - \frac{r}{R}\right)^2 + C_4\left(1 - \frac{r}{R}\right)^3$$

The constants C_2, C_3, and C_4 were determined to satisfy the boundary conditions of (1) a curve tangent at the outer rake position to the curve determined by the rake readings, (2) a prescribed mass flow, and (3) a curve which coincides with the outer rake points. The form of the equation inherently satisfies the zero velocity condition at the wall (assuming the density does not approach zero). The short-dash curves of figures 13 and 14 are drawn so that the total mass flow at the 1.278 model would give a mass-flow ratio of 1.00; and the long-short-dash curve is

that one where the integrated mass flow enclosed between the wall and the outer rake is equal to the "standard increment" applied in the general computations. The two curves coincide for the 4.026 model. The Mach number profile is then determined, since $M(r_o) \ll 1$, from

$$\frac{M(r)}{M(r_o)} = \frac{\rho U(r)}{\rho U(r_o)} \left[\frac{1 + \frac{\gamma - 1}{2} M^2(r_o)}{1 + \frac{\gamma - 1}{2} M^2(r)} \right]^{1/2}$$

$$\approx \frac{\rho U(r)}{\rho U(r_o)} \left\{ 1 + \frac{\gamma - 1}{4} M^2(r_o) \left[1 - \frac{\rho^2 U^2(r)}{\rho^2 U^2(r_o)} \right] \right\}$$

The effective Mach number, defined as that Mach number, which if invariant across the survey plane would give the measured values of mass flow, pressure, etc., of these runs were 0.209 and 0.219 for the 4.026 and 1.278 models, respectively. The average weighted pressure recoveries were 0.639 and 0.601.

The trace of the valve-position indicator was measured to an accuracy of 0.01 inch on the pressure record, which gave the indicated physical position of the valve to 0.005 inch. Some play in the linkage mechanism and change in the voltage applied to the slide-wire resistance reduced the accuracy of the position indicator for the large model. These factors were largely eliminated in the small model. There was also a lag of about 0.03 second in the response of the indicator so that for conditions of rapid throttling the valve readings were compensated for this time lag. The maximum valve speed obtained from the slope of valve position plotted against time was 0.55 inch per second.

In order to determine the values of static pressures and valve position at incipient buzzing mass flow, the corresponding values were read from the pressure-time or valve-position—time trace. Values were taken when either the high-speed motion pictures or the pressure traces showed instability. It was necessary to employ the motion pictures in some cases where the turbulence and hash level in the gages, especially the two forward ones, was high. The probable cause of the high hash level in the first two gages was separation in the subsonic diffusers.

Total amplitude measurements were taken by measuring peak-to-peak pressure fluctuations on the pressure-time curve.

The following are the estimated maximum probable errors arising when the flow is steady:

Mass-flow ratio:	
For high length-diameter ratios	±2 percent
For low length-diameter ratios	±3 percent
Valve position:	
For large model	±0.01 inch
For small model	±0.005 inch
Pressure recovery	±1.0 percent
Static pressure	±0.5 percent
Mach number in ram jet	±0.002

RESULTS AND DISCUSSION

General Results

Figures 4 to 12 show the performance curve of the inlets in terms of pressure recovery and mass flow. Experimental points having unsteady flow are denoted by flagged symbols. The ram jets with the higher value of length-diameter ratio were employed to give more accurate values of mass flow and pressure recovery for comparison purposes since in the larger models the velocity profile has become a smooth nearly symmetrical curve showing negligible effects of the center body wake and angle of attack by the time the rake station has been reached. Each of the high-length-diameter-ratio configurations is compared separately with its two counterparts, namely: the same length-diameter-ratio model of different diameter and the shorter version of the same diameter. It is obvious from inspection that the accuracy is lower in the lower L/D models, but the curves for the high and low L/D models of the same diameter and cowling-position angle may be considered the same within the order of the expected experimental scatter.

Table III is a compilation of the values of mass-flow ratio, pressure recovery, valve position, and ratio of static pressure to tank pressure at the start of buzz. The incipient mass flow, with one exception where the interval between the highest measured unsteady flow and lowest measured steady flow was large, was assumed equal to the largest value of mass flow at which unsteady flow was first recorded. This exception arose in the case of 1.278 - 14.91 - 48.1° configuration where the unsteady flow was noted up to a mass-flow ratio of about 0.89 and the lowest measured steady flow was at a ratio of 0.915. The critical

mass flow of 0.91 was determined by extrapolating a curve of pressure pulsation amplitude versus mass flow to zero amplitude.

The incipient pressure recovery was obtained from the faired curve of pressure-recovery mass flow at the incipient mass-flow value. The static-pressure—tank-pressure ratios and the valve positions, determined from the time-history records, are the average values of several runs.

Shadowgraphs of the critical flow shock pattern for the various model configurations are given in figure 15. These pictures, with the exception of figure 15(g) for a negative angle of attack, are of the high length-diameter configurations at a positive angle of attack of $1/2^\circ$. The shadowgraphs of the models are adjusted to have approximately the same dimensions to facilitate comparison. The cowling lip was referenced by two pieces of opaque tape affixed to the tunnel glass at the top and bottom of the test section, but because of the enlarging procedure just mentioned the tape will show only in the large-diameter-model pictures.

The external shock pattern for the configurations with cowling-position angles of 44.2° and 48.1° appear unaffected by the slight angle of attack. For the 44.2° configuration three-dimensional effects are responsible for the apparent presence of the normal shock ahead of the cowling when in reality it is just at the lip, a fact which may be verified by the opaque tape reference marks.

A difference in the flow configuration due to $1/2^\circ$ angle of attack is noticeable for a cowling position angle of 40.1°. The normal shock on the leeward side of the cross flow induced by the angle of attack is advanced ahead of the cowling lip more than the shock on the windward side; and, in addition, the leeward shock may terminate in a lambda shock near the cone. Proof that this phenomenon arises from the slight angle of attack is found in the shadowgraphs of the critical mass flow of the same supersonic diffuser configuration for an angle of attack of $+1/2^\circ$ (fig. 15(f)) and $-1/2^\circ$ (fig. 15(g)) which show the shock pattern to change with angle of attack. The cross flow of the boundary layer causes a boundary layer build-up on the leeward side which results in the asymmetric shock pattern.

Curves of Mach number at the center line of the rake plotted against steady-flow pressure recovery for configurations 4.026 and 1.278 - 29.82 - 48.1° are shown in figure 16. These curves are typical of the 44° and 40° configurations also. Values were not plotted for unsteady flow since such a procedure would make the plot multiple valued in pressure recovery.

Scale Effects

A dimensional analysis of the problem of testing buzzing models for correlation purposes yields the following results. The variables in the problem are: (1) pressure (p) or pressure perturbation (Δp); (2) stream velocity (V); (3) density (ρ); (4) length (L) or diameter (D); (5) viscosity (μ); (6) sonic velocity (a); (7) periodic time (τ); (8) turbulent velocity (w) and/or perturbation velocity (u). Then, the related nondimensional parameters in the mass-length-time system are: (1) Mach number $\frac{V}{a}$; (2) Reynolds number $\frac{\rho VL}{\mu}$, (3) wave length of model $\frac{L}{a\tau}$, (4) pressure coefficient $\frac{p}{\rho V^2}$ or $\frac{\Delta p}{\rho V^2}$, (5) turbulence or perturbation ratios $\frac{w}{V}$ or $\frac{u}{V}$. Thus, if models of different scale (L) are to be tested without maintaining constant Reynolds number, the effect of varying Reynolds number must be ascertained.

The importance of boundary-layer growth and separation to the stability of inlets in absence of combustion will be discussed in a later section of this report. If these viscous effects are to be a major factor in determining the stability of inlets, Reynolds number effects would then also be expected to be a major consideration.

Steady flow.- From the results presented the performance of the models to the start of buzz may be discussed. Figures 5, 6, 8, 9, 11, and 12, in which pressure recovery plotted against mass-flow ratio of model pairs having the same diameter and cowling angle are compared, show the performance of such pairs to be nearly the same within experimental scatter. There does appear to be a tendency for the lower L/D models to have up to 1 percent higher pressure recovery during buzzing, but this might be attributed to the different frequencies of the standing waves in the manometer tubing. Although the mass-flow measurements have a larger range of error in the low L/D models, the induction-gage pressures and valve-position indicator are not so affected. Hence, a good check of the conditions at start of buzz for the same diameter and cowling-position angle models is found in table III where the maximum variation of average valve position at start of buzz is found to be 0.005 inch and 0.01 inch for the 1.278- and 4.026-inch models, respectively, and of average static-to-tank pressure ratio at corresponding stations to be about 0.5 percent. An analysis of the high-speed motion pictures also revealed the shock patterns to be the same at the start of buzz independent of L/D ratio for the same diameter and cowling-lip angle.

A comparison of the performance of similar configurations having different diameters shows only a slight scale effect. The pressure

recovery mass-flow curves of the 44.2° and 48.1° diffusers (figs. 4 and 7) are nearly identical for the two diameters. Instability appears at a slightly higher mass-flow ratio in the larger model of 48.1° lip angle than in the corresponding small model, but the 2-percent variation has little significance. The shadowgraphs of the flow patterns at the incipient point for the above configurations (figs. 15(a) to 15(d)) show no important differences in the flow for the different sized models.

It is to be noted that in the 40.1° inlets where, although the critical mass flows are nearly the same, the peak pressure recovery, critical pressure recovery, and static-to-tank pressure ratio are higher in the small diameter model in spite of the lower Reynolds number of these models. See figure 10 and table III.

It was also found that the over-all incipient values did not change when the angle of attack was reduced to 0° or made negative by 1/2° for the configurations 1.278 - 40.1° although the local conditions alternated with the shock pattern. Shadowgraphs in figures 15(e) and 15(f) at a positive angle of attack are nearly identical for the different sized models. Figure 15(g) at an angle of attack -1/2° is not a mirror image of figure 15(f), although the tendency of the leeward shock to advance and bifurcate is quite evident. For a configuration such as this, which is extremely sensitive to changes in angle of attack, such a variation could be attributed either to a failure to exactly match the positive angle with its negative counterpart or to a slight eccentricity of the central body which would alter the effective angle of attack of the cone.

The Reynolds number effects on the profiles of the long L/D models are evident in figure 16 which are typical of the curves for all the cowling-position angles. Although both models have profiles of turbulent pipe flow the greater relative viscous forces in the low Reynolds number tests result in a larger region of retarded flow contrasted to the much more fully developed flow of the high Reynolds number model (fig. 13).

The velocity and mass-flow profiles of the low L/D models showed the influence of the 1/2° angle of attack in varying amounts in a majority of the runs. The pressure recovery and velocity were higher in that section of the survey plane behind the leeward cone surface for both large and small models. Two profiles for positive and negative angles of attack of configuration 1.278 - 14.91 - 40.1° showing the manner in which the asymmetry alternated with angle of attack are presented in figure 17. Oswatitsch (ref. 1) discovered the same phenomenon in certain of his tests at slightly larger angles of attack. Since the boundary layer tends to accumulate on the leeward side of the central body one might expect the poorer performance to occur in this region. For configurations 14.91 - 40.1° the shadowgraphs show external separation

on the leeward side as the incipient mass flow is approached. There are several possible explantions for the measured distribution of total pressure. First, the lambda shock on the leeward side might increase the total pressure recovery of the fluid flowing through the upper bifurcations sufficiently to offset the adverse effect of the separation at the cone surface. Secondly, the flow on the inner surface of the windward cowling might separate to a greater degree than that on the leeward side of the central body. Finally, there is the possibility of a more violent separation occurring in the subsonic diffuser, either off the central body or cowling surface of the opposite side. In other words, the early flow separation on one side of the center body may prevent a more violent separation of the flow on the same side later in the subsonic diffuser.

The apparent lack of a strong Reynolds number effect in determining the stability of the 40.1° and 48.1° configurations (where the conical shock did not intersect the cowling lip) was not expected. Prior to conducting the tests it was thought that the Reynolds number effect would be small for those inlets which had the conical shock at the lip since the vortex sheet position would govern stability. For those inlets in which the central-body boundary layer was an important part of the governing mechanism for stability, the Reynolds number was thought to be a very important parameter. This negligible effect of Reynolds number should not be assumed to apply to inlets in general, but rather to represent the effect only on the particular configurations investigated. It does, however, show that there is the possibility of testing cold-flow scaled models for approximate prediction of stability limits.

Unsteady flow.- The behavior of the comparative models during buzzing was also very similar. This similarity extended not only to the unsteady-flow cycles which were made up of multiple waves but also to the cycles dependent on random pulses. Typical examples of the first case are shown in figure 18 where the pressure-time curves of configuration 1.278 - 14.91 - 44.2° at a mass flow ratio of 0.69 is compared to the curves of configuration 4.026 - 14.91 - 44.2° at a mass flow of 0.66. In spite of the 3-percent variation in mass flow it is obvious that the wave forms are quite similar if the time scale is modified by a factor equal to the length ratio. The 1.278 model pressure records were taken at a higher film speed to facilitate comparison. The vertical lines on the record indicate time intervals of 0.01 second.

Figure 19 shows the pressure-time curves of configurations 14.91 - 40.1° near the start of buzz where there is no regular cycle buzzing, instead the unsteady flow is characterized by spasmodic pulses separated by time intervals of various lengths. These latter curves show the unsteady behavior to be similar, even where irregular.

The unsteady flow of configuration 1.278 - 14.91 - 40.1° was unstable at a mass-flow ratio of 0.72 and, as is shown in figure 20, changed from a relatively low frequency of 120 to 160 cycles per second, which was often found in most of the 1.278 - 14.91 configurations, to much higher frequencies, usually approximately 800, 900, or 1,400 cycles per second. The whole shock pattern oscillated at this frequency. With no change in valve position this high-frequency pattern would in time break down and revert back to the low frequency, etc. This conversion to high frequency is shown in figure 20. In figure 20(b) (gage 1 is inoperative) there is no valve motion and the high frequency of 900 cycles per second is superimposed on the 160-cycle-per-second buzz. In figure 20(a) the valve is slowly closing to the position of figure 20(b), and in this case the high-frequency breakdown results in a 1400-cycle-per-second buzz with the elimination of most of the low-frequency pulses. An examination of other records and motion pictures at slightly higher mass flows showed a possibility that the frequency of oscillation of the bifurcated part of the shock to be about 900 cycles per second when the upper part of the shock was responding to the low frequency.

Figures 19 and 20 also prove the fact that the buzzing cycles are not necessarily repeatable, but that single pulses may occur or the cycle change drastically with no change in ram-jet geometry. Averaged results for the high and low frequency, obtained with no valve motion, similar to that in figure 20 showed a variation of less than 1/2 percent in pressure recovery and mass flow which is less than the scatter of the tests.

The flow of the longer 1.278 - 40.1° model did not break down completely into a high-frequency oscillation for periods longer than 0.02 second, but the pressure records did show evidence of such high frequency which was usually definitely subordinate to the low frequency. Previous unpublished data of tests at the Langley Aeronautical Laboratory have, however, shown the high-frequency oscillation to be present in high L/D models. Safety considerations, plus the doubt that large amplitude oscillations would be free from influence of the test-section boundaries, prevented all but a few runs of large pulsation amplitude for configuration 4.026 - 40.1°. No runs for the 14.91 L/D model were made at a low enough mass-flow ratio for the high frequency to appear predominant, though the oscillation frequency of the lambda shock was determined to be about 350 cycles per second compared to the 900 cycles per second of the model smaller by a factor of 1/3. A few runs were made at low mass flows for 4.026 - 29.82 - 40.1° and these also had high-frequency components subordinate to the low frequency.

Figure 21 is a portion of an 850-frame-per-second shadowgraph motion-picture film taken concurrently with the pressure record shown in figure 19(b) of a single spasmodic pulse of configuration 1.278 - 14.91 - 40.1°. The shadowgraph frames are numbered to correspond to the numbers on the pressure record.

From these shadowgraphs it is evident that an appreciable part of the total shock motion, as well as almost all of the lambda shock motion, occurs between frames 9 and 10. This is in agreement with the pressure record of the gage at $x/L = 0.275$ which shows, more sharply than the other gages, the break in pressure which for this particular gage occurs concurrently with shadowgraph frame number 10. The time lag, or time for a wave to travel from the cowling lip to $x/L = 0.275$, is about one-half the time between frames. Thus, in this case, where it should be emphasized there was no valve movement whatsoever, it is evident that the over-all ram-jet geometry can have no effect on the initial shock motion. This is substantiated by the fact that the initial shock motion, which is an appreciable part of the over-all motion, has been completed before any waves which it generates at the inlet have had time to even travel 4 diameters downstream, let alone have had time to reflect from any significant geometrical or aerodynamic changes and return to the cowling to influence further motion. The reflection from the valve of the start of the initial expansion reaches the inlet at frame 12, but the shock does not start to retreat until frame 19 although expansion waves reflected from the nozzle are continuously hitting the shock during the interval between frames 12 to 19. The fact that the shock does not start to move rearward when the reflected expansion from the exit nozzle strikes it from behind indicates that there must be a flow phenomenon at or near the cowling which generates compressions to cancel the effect of the expansion. The above shock motion is not peculiar to this particular configuration but has been observed to occur in other tests. Although many of these tests may have a gradual throttling process, it is found that the shock is still out of equilibrium with the rearward part of the ram jet (that is, it moves faster than the low throttling rate would require).

Note also that the normal shock is slightly further advanced than the position of figure 15(f) at the incipient mass flow. Thus for a short period of time the shock has an equilibrium position at a mass flow below the value for start of buzz.

The model pairs having the same diameter, supersonic diffuser, and subsonic diffuser configuration have approximately, within the expected maximum error, the same pressure recovery mass-flow curves (figs. 5, 6, 8, 9, 11, and 12). In the unsteady flow range there does appear a slight tendency for slightly higher pressure recoveries for the shorter L/D models. Now only the combustion-chamber volume varies in these comparable pairs. Since the combustion-chamber volume changes by a factor of about three between the 29.82 and 14.91 L/D models, according to the resonator theory of reference 7 the slope of the pressure recovery against mass flow curve at the start of buzz for these configurations with continuous slopes should also vary so that the slope of the 14.91 L/D model should be three times the slope of the 29.82 L/D model since the absolute values of pressure recovery and mass flow at start of buzz

are the same (table III). However, the experimental curves for the 40.1° and 48.1° configurations having continuous slopes show that the low L/D models generally have a smaller, not larger, slope.

Discussion of Stability Criteria

Since various contrasting theories (refs. 5 to 7) have been expounded regarding the start of instability of supersonic diffusers, there is a definite need for clarification of the subject. It will be advantageous to consider first the basic aerodynamic phenomena involved in the initiation and continuation of the buzz cycle.

Quasi-one-dimensional theory for originating mechanism.- The theory of reference 6 describes the buzzing cycle once it has been initiated, assuming the initiating mechanism to be some form of separation near the inlet. It was found that an unsteady-flow theory based on a quasi-one-dimensional analysis gave very close correlation to the experimental pressure-time records in the ram-jet model. The shortest model studied, with an L/D of about 16, was rather long for a ram jet; however, since the gage nearest the cowling, located about 5 diameters downstream from the cowling, showed excellent agreement with the plane wave theory, it may be assumed that plane wave theory holds for ram jets having L/D greater than 5 and probably even to lower values.

On a quasi-plane wave basis the buzzing cycle may be analyzed in the following manner: In the start of buzzing the normal shock moves outward away from the cowling and this shock motion requires compression waves striking the downstream side of the shock. Since the pressure-time curves of reference 6 and figure 19 show that in the absence of rapid throttling there are no compression waves moving upstream inside the ram jet at any appreciable distance from the inlet, then the required compression waves must be generated at or near the cowling entrance. Equation (2) of reference 6 shows that either a flow area decreasing with time or a flow entropy increasing with time is needed to generate upstream moving compression waves (that is, an increase of the parameter Q in eq. (2) of ref. 6). A separation, or even an unseparated boundary layer growing with time, satisfies both these requirements since the rate of displacement thickness growth produces a decreasing effective flow area while concurrently the entropy is increasing due to boundary-layer losses.

The entering of the vortex sheet from the conical-normal-shock intersection into the cowling will also result in both a reduced flow area for the flow inside the vortex sheet and, after mixing, an increased entropy. Moreover, the entrance of the vortex sheet must be violent and abrupt since the vortex sheet itself cannot stagnate on either the outer or inner surface of the cowling due to the total pressure difference

existing across it. Thus, the entrance of the vortex sheet or the growing of the boundary layer (separation) have much the same effect as closing a throttling valve located near the inlet.

Thus, the mechanism of buzz initiation may be described as follows: The entrance of the vortex sheet, increasing separation, or boundary-layer growth (behind the shock), either on the central body or on the inner surface of the cowling, generates a compression wave which forces the normal shock outward. This initial growth may be very small and may result from the random fluctuations present in the flow. Such a case was illustrated in figure 19 for no valve motion. When buzzing arises during throttling, the compression waves generated by the throttling process force the shock to a position where either a random pulse at the inlet or the next small wave from the exit throttle may perturb the shock. In cases where the entrance of the vortex sheet into the cowling causes the initiation of buzz, the pulse generated by the abrupt motion of the vortex may also be augmented by separation on the cowling surface so that the compression wave generated is stronger and consequently the shock is generally forced out abruptly. Reference 5 explains the case in which the vortex sheet enters the cowling without causing separation as resulting from the mixing of the low and high energy air on each side of the vortex sheet before attempting subsonic diffusion. In addition, the pulse created by the vortex motion would be weakened for the inlets having sharper leading edges and thinner cowling thicknesses. These possibilities could explain the observed entrance of the vortex sheet into the cowling without causing buzz. In cases where separation on the central body initiates the buzz there is usually no such rapid growth of the separated region, instead a small growth of separation generates a compression wave which forces the shock out slightly. However, in this new forward position to which the shock has been forced, new flow conditions exist behind it which include a more adverse pressure gradient between the shock and the cowling entrance. Consequently, additional separation may occur with consequent production of more compression waves to force the shock out farther, etc. This outward motion of the shock will continue until either (a) an equilibrium condition is reached in the region of flow between the shock and separation region, or (b) an expansion wave can strike the shock from behind to lower its back pressure so that it will retreat toward the cowling (see ref. 6).

It is to be noted that it is not necessary to "choke" the entering flow in the sense that sonic velocity must be obtained near the cowling entrance to start buzzing. The rate of effective flow area decrease and entropy increase are the important parameters, though it must also be emphasized that these factors will generate stronger waves when the Mach number is near unity.

Wave cycle.- Now that the basic phenomena involved in the initiation of buzzing have been described, the mechanism by which it is perpetuated

will be reviewed (see ref. 6): The outward motion of the shock and the increasing boundary-layer displacement thickness reduce the mass flow through the diffuser. This reduced mass flow results in an expansion wave which moves down the subsonic diffuser and combustion chamber and lowers the pressure, density, and velocity. At the sonic exit nozzle, this downstream expansion is reflected as another expansion wave which moves upstream until it meets the shock. Whereupon the shock moves rearward and passes through the position it had at the start of buzz. The separation which originally caused the buzz is not as large at this time because the upstream expansion wave creates a favorable pressure gradient and the retreating shock results in reduced losses. In other words, as the shock passes the position from which buzz started the flow conditions are not the same. A change in flow pattern at the same shock position is shown in the instantaneous shadowgraphs, figure 22. Since the lambda pattern is known to exist in the outward motion, the other flow configuration probably occurs during the retreating shock motion. This would also be in accord with the effect of favorable pressure gradient just mentioned. The rearward shock motion generates a downstream compression wave, which in turn reflects as another compression wave moving upstream until it also strikes the shock.

In certain cases, since the strength of the waves reflected at the nozzle depends on the relative constriction of the nozzle area to combustion chamber area, this reflected compression is strong enough to return the shock to the position at which buzzing began, and consequently another cycle starts immediately. The frequency is then nearly identical to that of an organ pipe closed at one end with a length equal to the ram jet.

In other cases the first reflection is weaker so that the shock is not moved far enough forward to reach the buzzing position. However, since the compression wave-shock wave interaction results in the generation of a downstream compression which is in turn reflected at the nozzle as an upstream compression wave; this latter wave may move the shock out far enough for the next cycle to commence. If not, further compressions are generated and reflect until the shock is finally forced upstream to the point where it initially started to buzz. Reference 6 proves this behavior by extremely close correlation between theory and experiment.

There are also cases where a reflected compression wave in itself is sufficient to push the shock ahead of its initial position, in which case the shock will move farther out in the next cycle than it did in the previous one. In this manner the amplitude of the oscillation may increase from its original one without further throttling.

In cases of a very high frequency buzz (such as shown in fig. 20) which generally occurs at the lower mass flows of certain inlets there

is insufficient time for any wave whatsoever to traverse the ram jet in the period of one cycle. Consequently the "source" of the buzz must be the flow in the immediate vicinity of the inlet, although the alteration or amplification of these pulses may depend on the over-all ram-jet flow. In other words, the shock and boundary-layer oscillations ahead of the ram-jet ducting may be compared to a turning fork at the mouth of an air column. For example, the oscillation frequency of the foot of the shock of configuration 1.278 - 14.91 - 40.1° appeared to be about 900 cycles per second while the remainder of the shock pattern oscillated at a much lower frequency. Since the fifth harmonic (second and fourth do not exist) of the ram-jet ducting acting as an organ pipe closed at one end is about 870 cycles per second it is not at all surprising to find high-frequency buzzing in the range of 800 to 900 cycles per second as described previously. A possible explanation for the mechanism of the "source" of the buzzing is the fact that the "normal" shock, which is in motion due to separation in its rear, will move far enough forward so that the cone boundary layer existing at its foot becomes small enough and possesses enough momentum to be able to withstand the pressure ratio of the shock without separating, or at least without separating as much. Now since it is the rate of increase in separation, boundary layer, or entropy which causes the upstream moving compression waves which keep the shock in motion; when this rate falls off, resultant expansion waves will travel upstream to start the shock moving rearward again. As the shock moves rearward the boundary layer becomes more susceptible to separation and a point is reached where the rate of change of the aforementioned variables become positive and the next cycle commences.

Proposed theory for stability criteria of supersonic inlet in cold flow.- It has been shown for axisymmetric conical center body supersonic inlets without heat addition that the pressure disturbances (in the absence of rapid throttling) originate at or near the cowling entrance. Furthermore, the sound wave traveling downstream and carrying the "news" of the initiation of buzz reaches the combustion chamber only after the second shock has completed a substantial part of its outward motion. Consequently, in these cases it is impossible for the mechanism which determines the stability to be located in the combustion chamber (in cold flow); instead one is forced to look for the answer in the forward part of the ram jet at the supersonic diffuser and that part of the subsonic diffuser just behind it near the cowling entrance. It must also be noted that although the flow inside the ram jet may be very closely approximated by quasi-one-dimensional steady or unsteady flow, as in reference 6, the flow external to and ahead of the cowling cannot be so treated. The pressure pulses emerging from the cowling spread out into the whole region of flow behind the normal shock and are not "bound" by the streamline entering the cowling.

With these points in mind, a possible explanation of the phenomenon may be examined qualitatively by considering the external flow ahead of

the cowling. An insight into the over-all reaction can be obtained by assuming quasi-one-dimensional flow although it must be remembered the flow ahead of the cowling is three-dimensional. In the one-dimensional-flow model, the stream tube entering the cowling is considered as a "channel" with flexible walls which expand at a rate sufficient to account for the spillage of mass flow around the cowling in the actual flow. Furthermore, any changes from the unperturbed state of entropy ahead of the cowling are assumed to occur not at the shock system but at the cowling. In other words, a distortion is introduced by considering that all of the generated waves are created at the cowling instead of in the whole region between the shock and cowling. The phenomena of increasing separation or boundary-layer thickness which generate upstream moving compression waves and create conditions of reduced mass flow and higher stagnation pressure immediately behind them have been discussed. Now with the concept of a perturbation (that is, vortex entrance, increased boundary layer, separation) which decreases the effective flow area and increases the entropy at the cowling entrance so that an upstream compression wave is generated at the inlet, the conditions for stability may be determined:

(a) Stable condition: If, as the shock is forced outward with decreasing mass flow, the expansion waves generated by the flexible walls (spreading out to accommodate the three-dimensional spillage) are of greater strength than the net sum of the initial compression wave and any additional waves generated at the cowling due to flow changes arising from the perturbed shock, then the shock will halt its outward motion and retreat toward the cowling. It should be noted that both a decrease in entropy rise through the shock system as well as a decrease in separation or boundary-layer thickness in the flow just after the shock (both conditions are associated with an increase in the conventional total pressure recovery) will result in the generation of expansion waves to aid those arising from the flexible wall in forcing the shock to retreat.

(b) Unstable condition: If, as the shock is forced outward with decreasing mass flow the expansion waves generated by the flexible walls are of less strength than the net sum of the initial compression wave and any additional waves generated at the cowling, then the shock will not immediately halt its outward motion. Instead it will move ahead of the cowling until it reaches an equilibrium with the flow in the cowling (that is, the conditions behind the last wave originating at the cowling are matched by a particular shock position) or until the net expansion wave (that is, the cumulative wave) generated on the downstream side of the separation "throttle" has an opportunity to reflect from the exit nozzle and return to the inlet. Both type of shock motion are demonstrated for the same diffuser configuration with different combustion chamber lengths in figures 9, 10, 15, and 16 of reference 6. Again it should be noted that an increase in entropy rise through the shock system and an increase in separation or boundary-layer height (corresponding to

a decrease in the conventional total pressure recovery) will result in the generation of additional compression waves to help keep the shock in outward motion.

With these arguments in mind it is evident the stability of a supersonic inlet is determined by the relation between the transient flow conditions behind the normal shock and the instantaneous flow existing in the cowling inlet of a conical diffuser. The fact that buzzing has been found experimentally to arise concurrently with a positive slope of the mean (time averaged) pressure recovery versus mass-flow curve (ref. 7) does not conflict with the above analysis. Moreover, since the instability criteria proposed previously in this section show that an instantaneous decrease in pressure recovery with mass flow at the inlet will generate destabilizing compression waves it would be surprising if the instantaneous values integrated over a buzzing cycle and then averaged did not yield values lower than the steady-flow value at the last stable position.

A similar stability criterion based on separation or boundary-layer growth could be applied to scoop inlets. Instead of the dependence of stability on the boundary-layer effects on the central body and cowling in the case of symmetric conical inlets, the dependence would be based on the boundary layer on the compression surface and the opposite wall.

The buzzing of convergent-divergent perforated inlets (ref. 3) might also be explained on a similar, but less complicated, basis. Owing to lack of pressure-distance-time data it is impossible to definitely state the disturbance origin, but the following probable solution is presented. In contrast to the conical inlets where separation on the central body or inner cowling surfaces was the triggering mechanism, for convergent-divergent perforated inlets the probable mechanism is the thickening of the boundary layer on the outside of the cowling.

When a shock is located in the converging section of the inlet the mass flow passing through the shock is equal to that passing through the rearward perforations and through the throat. Now along the outer surface of the cowling the boundary layer thickens abruptly at the position of the internal shock because of the shock pressure differential which is transmitted through the perforations and also because of the increased mass-flow spillage through the perforations behind the shock (see fig. 19 of ref. 3). This thickening of the boundary layer causes an oblique compression wave to propogate into the free stream so that the pressure in this region is above free-stream static.

Now if a momentary thickening perturbation of this external boundary layer occurs, then the effective "ramp angle" of the layer will increase and the oblique compression wave increases in strength, the pressure increases, and the increasing pressure on the outer side of

the perforations decreases the mass flow through them. The effect of pressure on the mass flow may be verified by the appendix of reference 3.

The reduced mass-flow spillage means that there must be an increase in the mass flow through the throat, but this is impossible without shock motion since the throat is choked at the original shock conditions. The shock must then move forward seeking to find another equilibrium condition matching the flow through the perturbed shock with the perturbed flow through the throat and perturbed spillage. As the shock moves upstream (usually) into regions of higher Mach number the losses across the shock will increase so the stability will depend upon whether the spillage flow can be increased enough to pass the added required mass flow. The external pressure is also increasing as the shock moves up because of increased shock strength and more spillage to produce a larger boundary layer with resultant stronger oblique compression waves.

In this case the stability of the inlet would then hinge on the perturbed relationship of mass flow through the throat and perforations and still be divorced from steady-state combustion-chamber pressures. The remainder of the buzzing cycle would follow and depend on reflections from the exit nozzle.

Discussion of Ferri-Nucci vortex-sheet theory.- The stability theory (ref. 5) based on a vortex sheet impinging on the cowling lip was found to be valid for the 44.2° configurations. Since the conical shock intersected the cowling lip, the vortex sheet struck the lip as soon as the normal shock emerged from the cowling and prevented any steady mass-flow reduction below the maximum attainable for this configuration. However, for cowling angles of 40.1° and 48.1° there was no vortex sheet approaching the cowling at the onset of buzzing and hence this criterion was not applicable in these cases. The instability of these two models arose from separation on the central body at the foot of the shock. Since the cone surface Mach number was high (approximately 1.4), the pressure rise across the "normal" shock should be appreciable and separation should be expected. Thus, the vortex-sheet criterion appears to be inapplicable for inlets with high Mach numbers on the cone surface unless the vortex sheet at critical mass flow is quite near the cowling lip.

Other investigators have arrived at similar conclusions. The vortex criteria may also become fallible for inlets having very low rates of subsonic diffusion after the cowling lip.

Discussion of Sterbentz-Evvard resonator theory.- The theory of reference 7 is based on an analysis of the oscillation in the ram jet which considers a resonator model similar to that which might be obtained from a system composed of a mass with a weightless spring at each end. The "mass" is a "slug" of air in which compressibility is neglected and which

is located in the diffusing region of the ram jet. This slug is assumed to oscillate as a unit parallel to the axis of the ram jet so that a region of "virtual separation" arises between the lateral boundaries of this slug and the diverging surfaces of the diffuser.

One of the "weightless springs" is the remainder of the air in the ram jet (mainly the air in the combustion chamber) where compressibility effects give rise to pressure changes to provide a force-displacement relationship. The pressure changes are assumed to result from the variation in the amount of air present in the combustion chamber as the flow of air entering from the diffuser and that leaving the choked-exit nozzle vary with time. The inertia of the air in the combustion chamber is neglected. The assumption is also made that the pressure in the combustion chamber may be considered constant throughout at any instant.

The other weightless spring is the external shock pattern which gives rise to pressure changes exerting a force on the upstream end of the slug. This spring has a spring constant that may be either positive or negative. It is assumed that total pressure, in lieu of static pressure, at the inlet produces accelerating forces. Furthermore, the variation of this total pressure from a mean value is assumed to be given by the product of the variation of the subsonic diffuser exit-mass flow from a mean value and of the mean slope of the curve for subsonic-diffuser-exit total pressure against diffuser-exit mass flow. In other words, it is assumed that the dynamic performance of the supersonic diffuser is equivalent to the mean (that is, quasi static) performance of the supersonic and subsonic diffuser combination.

The assumptions of constant density throughout the slug and constant pressure at any instant in the combustion chamber is equivalent to assuming that the wave length of the highest frequency component of the oscillation is much larger than the length of the ram jet. If the high-frequency components are to be ignored and only fundamental vibrations considered then the ram jet must have a length negligible compared to the fundamental wave length.

Since reference 6 has proven that quasi plane waves govern the buzzing cycle, it will be advantageous to attempt a correlation between these waves and the resonator model. The downstream spring is an approximation for the effect of the moving plane waves including those reflected from the choked exit nozzle. The upstream spring then should be chosen as an approximation for the effect at the cowling of the waves traveling upstream as well as reflecting from the shock system and boundary layer at the cowling. However, by assuming the upstream "spring constant" to be given by mean values of the slope of the total pressure versus mass-flow curve measured at the subsonic diffuser exit, the approximation becomes dubious.

The oscillating slug of air in the diffuser neck is used to approximate the fluid in the ram jet which has the highest velocity perturbations. The plane-wave theory shows the choked exit nozzle assumption results in the ram jet acting much the same as an organ pipe closed (in regard to perturbations) at the exit so that the velocity perturbations are highest near the entrance. However, when the combustion chamber is much longer than the diffuser, the momentum perturbation in the combustion chamber cannot be neglected.

Now if the frequency of oscillation is low and of a simple harmonic type without higher frequency components so that the wave length of the oscillation is much larger than the length of the ram jet, then the relative pressure distribution along the ram jet at a particular instant of time, obtained by quasi-plane-wave theory, may be crudely approximated by the resonator model. Thus, under these conditions, the resonator model might be expected to give frequencies of the correct order of magnitude.

However, this resonator model would still be inapplicable for the determination of the correct stability parameters. The reason for the possible usefulness on one hand for frequency computations and the unsuitability for stability computations on the other hand lies in the importance of time effects and local flow conditions on stability.

It has been shown previously that the flow perturbations at the start of buzz originate at the inlet and grow to an appreciable size relative to their ultimate magnitude before the waves generated by the start of the growth can travel downstream to the combustion chamber. If waves traveling downstream with a speed equal to the sum of the sonic and the fluid speeds reach the combustion chamber only after such an appreciable growth, then it is obvious that any entropy discontinuities, which move with the speed of the fluid and which arise from the shock motion or boundary-layer variations at the cowling must arrive at the combustion chamber at an even later time. Thus the springs of the resonator model, which approximate (for frequency purposes) the effect over a complete low frequency cycle of the waves in the ram jet, are not applicable at the start of buzz since the upstream waves are not present in the actual physical phenomenon.

If one were to set up a "mass and spring" model for stability purposes as an analogy to the stability criteria proposed in an earlier section of this report, the mass would be the slug of air between the normal shock and the boundary layer or entropy disturbance near the cowling inlet which gives rise to the upstream moving compression waves. The upstream spring would exert a force related to the instantaneous value of pressure recovery and mass flow through the shock and cowling system. There would be no downstream spring for stability determination since, as proved previously, the initial motion of the slug would be

unaffected by reflections from the rear of the ram jet. However, instead of the downstream spring acting on the rearward surface of the slug, there would be a forcing function representing the waves generated by the boundary-layer disturbance. The initial motion (stability) of the slug would then depend upon the relation between the forces exerted by the upstream spring and forcing function, where the forcing function is also affected by "feedback" of a magnitude dependent on the slug position. In this analogy the feedback forces represent the additional waves generated owing to changes of entropy, effective flow area, and spillage at the cowling inlet as the shock is displaced from its original position. The stable case would then occur when a random force arising at the rear face of the slug would move the slug only slightly before the spring ahead could stop the motion. The converse would then be true for cases of instability in which case the slug would continue to move outward until stopped by removal of the forcing function or (if enough time has elapsed in the equivalent ram jet to permit reflections from the exit nozzle) the application of another restoring force to the rear face.

The various assumptions employed in the resonator theory of reference 7 should also be weighed closely. The very critical assumption that the pressure on the upstream face of the slug can be given by a mean relation between total pressure recovery and mass flow at the diffuser exit is particularly susceptible to doubt. First there is the question of the indeterminancy of the slope of pressure recovery versus mass flow for inlets, operating with the conical shock at the lip of the cowling, which have no reduction in mass flow without buzzing. The slope of the curve is then discontinuous at the start of buzz (see fig. 7). Then there also arises the question of the relationship of static to dynamic properties. For example, if the shock velocity may be considered slow then the mass flow entering the cowling would be the same for similar cases to those shown in figures 22(a) and (b) and figures 22(c) and (d) where the shock pattern is quite similar except for the bifurcation at its foot. However, the similarity of pressure recovery in the combustion chamber could be markedly affected by the varying degrees of separation at the foot of the shock even though the mass flow was the same. If the shock velocity may not be considered slow, then there immediately arises a discrepancy in the assumption since the pressure recovery is different across advancing and retreating shocks when the mass flow behind them is the same. In addition, the assumption that the instantaneous static pressure at the inlet may be approximated by the quasi-steady total pressure at the diffuser exit not only ignores compressibility at the inlet (where the Mach number is high) but also disregards possible strong changes in the performance of the subsonic diffuser as the shock moves outward (usually) accompanied by separation either on the cowling or center-body surface.

Finally, there is the question whether it is correct to use mean values to describe quasi-steady-flow conditions for part of a cycle when

there is never any possibility of equilibrium between the different parts of the flow. In other words, if strong waves or disturbances exist at any instant between the cowling and the subsonic diffuser exit, then the pressure perturbation at the cowling cannot correctly be approximated as the product of the mean slope of the diffuser exit pressure-recovery mass-flow curve and diffuser exit mass-flow deviation from the mean. For example, for the configuration of figures 9 and 10 of reference 6 from the instant the first cycle of buzzing begins (with the normal shock at the cowling inlet) the conditions just behind the shock never reach an equilibrium with those at the inlet until the shock finally halts its motion and remains steady two-thirds of the way out on the spike. In other words the aforementioned equilibrium is never attained so that the quasi-steady state never exists with the shock a quarter of the way out, half the way out, etc. Yet a mean value as employed in reference 7 presumes that the flow is in equilibrium as it passes outward along the spike and that possible steady flows exist a quarter of the way out, half the way out, etc.

The neglect of the velocity perturbations in the combustion volume, when the combustion chamber is long relative to the diffuser length, must also be considered since the ratio of the combustion chamber area to "slug" cross-sectional area is usually between three and four. Thus neglecting these combustion-chamber perturbations relative to those in the slug roughly assumes that one-third or one-fourth is negligible compared to unity.

The wave length of the oscillation and its higher frequency harmonics in relation to the dimensions of the model must also be examined. For example, for the higher frequency oscillations of references 7, 9, and a British paper by C. F. Griggs and E. L. Goldsmith (not generally available), the wave length of the basic oscillations are only five to six times the length of the model (i.e., an equivalent n between 2.5 and 3) so that the constant pressure and density assumptions become inaccurate.

It should be noted that the resonator theory cannot possibly be applied to the very high frequency buzzing discussed in a previous section of this paper and in the British paper. The wave length of the high-frequency oscillation in the latter paper, where the L/D ratios of the models were approximately 3 to $3\frac{1}{2}$, was only twice that of the model. The highest frequency oscillation of configuration 1.278 - 14.91 - 40.1° had a wave length of less than half the model length. Furthermore, the resonator theory of reference 7 cannot account for an abrupt change in frequency of any significant magnitude with no significant change in valve position, mass flow, or pressure recovery.

Experimental data are compared with the resonator theory in references 7 and 9 as well as in the British paper. The experimental

frequencies agree in regard to trend and order of magnitude. The arbitrary value of the geometric parameter denoting the end of the oscillating slug was chosen by Griggs and Goldsmith to give a minimum resonator frequency; yet the experimental values were always lower than the resonator frequency (except for the very high frequency cases) and errors ranged up to 50 percent of the experimental frequency. It should be noted that when the wave length of the oscillation was about five or six times as great as the ram-jet length, Griggs and Goldsmith reported theoretical frequencies consistently higher than experimental values whereas references 7 and 9 found theoretical frequencies to be lower than experiment. Since a linearized theory, when stretched to the limits of its applicability, usually gives results consistently on one side of experimental data this irregular behavior is at present unexplainable.

The comparison between the slope of the diffuser pressure recovery versus mass-flow curve at start of buzz predicted by the resonator theory and the experimental values of reference 7 and others is not conclusive. Griggs and Goldsmith state the magnitude of the slope to be so small for the models tested that the criterion of a positive slope appears to be sufficient for instability. The data of reference 7 indicate buzzing to occur with a positive slope, but the magnitude of the experimental slope sometimes exceeds and at others is not as large as the theoretical slope.

It should be noted that there are major differences between the instantaneous relationship involving total pressure and mass flow at the cowling which was employed as a stability criterion in a previous section and the mean relationship obtained from the resonator theory of reference 7. First, the mean relationship is concerned with the whole-ram-jet geometry while the instantaneous one is concerned only with conditions local to the cowling. Secondly, changes in the combustion-chamber total pressure are the result of buzzing while the instantaneous variation at the cowling is a requisite condition for instability. The separation "throttling" and reduced mass flow generate expansion waves moving downstream into the combustion chamber which reduce the total pressure, and of course these waves are later followed by fluid of higher entropy. The fact that buzzing occurs only with a positive slope of the mean total-pressure versus mean mass-flow curve has been explained in a previous section as resulting from a cyclic integration of the effect of the waves and entropy increase.

The amplitude computations of reference 9 are based on the same model as the frequency computations with the exception that the upstream spring "constant" may be nonlinear and is determined as the slope of an assumed steady flow relation between diffuser pressure recovery and mass flow. Thus these computations might be expected to also yield results showing the general trends and orders of magnitude. It has been stated previously in this paper that the quasi-plane-wave solution for certain

frequencies might be approximated by constant pressure in the combustion chamber at any instant of time. However, there is a variation in amplitude along this chamber which can be significant for amplitude considerations at higher frequencies. An examination of the experimental data of figure 4 of reference 9 reveals several facts pertinent to this argument. First the higher frequencies of each of the long and short models are inversely proportional to the model lengths which substantiates the fact that quasi plane waves govern the oscillation. The wave length of the particular oscillation is about $5\frac{3}{4}$ times the length of the particular ram jet ($n \approx 2.9$). Now the experimental amplitudes were measured at different values of $\frac{x}{L}$($x/L \approx 0.8$ for small models, $x/L \approx 0.5$ for large) and consequently since quasi-plane-wave theory predicts and experiments show amplitudes increasing with x/L it is to be expected that the measured amplitudes would be higher for the shorter model. If the gages had been located at the same value of x/L the amplitudes could be nearly equal. The result obtained by the resonator method which predicts higher amplitudes for the shorter model may be interpreted to reflect the fact that the longer combustion chamber length relative to total length of the larger volume ram jet yields an average pressure amplitude over that length which is less than the average pressure amplitude over the shorter relative length of the small-volume ram jet (since these lengths are taken from the exit of the ram jet and local amplitude increases as the exit is approached).

In conclusion it may be stated that the model assumed in the resonator analysis of references 7 and 9 may be considered a rough approximation to the actual phenomena when applied for purposes of obtaining the general trends and orders of magnitude of frequency and amplitude of oscillation providing the wave length of the highest frequency component of the oscillation be much larger than the length of the ram jet. The resonator analysis is not applicable when considering the initial stability of the inlet without combustion and should not be so applied to obtain such stability criteria.

Comparison Between Theoretical and Experimental Pressure Amplitudes and Mass Flow

The theoretical approximation to determine pressure amplitude variation with mass flow was applied assuming the shape of the pressure-time curve at $x/L = 1$ to be either sinusoidal or sawtooth with equal time intervals between peaks and valleys. The sinusoidal form is often found experimentally for the lower amplitudes. As the buzzing becomes more violent, the general form of the pressure-time curve usually becomes more highly peaked so that a sawtooth curve more nearly approximates the

actual curve. Of course, the experimental pressure records at higher amplitudes are usually made up of many superimposed waves, but these also can be approximated by adding simple curves. For example, figure 23 compares the pressure-time curve obtained experimentally for configuration 1.278 - 14.91 - 48.1° to the one obtained by adding a sinusoidal curve with $n = 1$ to a sawtooth curve with an equivalent $n = 3$ and amplitude about four times that of the sinusoidal curve, (that is, sawtooth curve has a frequency one-third that of the sinusoidal curve). The small perturbation pressure amplitude theory permits the addition of such pulses since the governing differential equation (eq. (8)) is linear; but it cannot predict the relative amplitudes of the waves having different frequencies without making some assumption regarding how much of the decrement in mass flow is due to each particular wave. Then a further assumption would be necessary regarding the phase relationship of the waves in order to obtain net peak values. Since there is no simple way of estimating these factors, they are ignored and the amplitudes computed as if the whole pressure and mass-flow variation were due to the lower frequency (higher value of n) oscillation. Note that the $n = 1$ oscillation has a very small amplitude near the midpoint of the ram jet (see gage 3 at $x/L = 0.602$ of fig. 23) the approaches zero as $x/L \longrightarrow 1/2$, $m_b \longrightarrow 0$.

The variation of pressure total amplitude coefficient with axial position along the ram jet for a value of $M_b = 0.14$ is shown in figure 24 for both the sine curve and sawtooth curve. The sawtooth curve predicts amplitudes from 0 to 20 percent higher, other conditions being equal.

The variation of total amplitude coefficient with incipient Mach number is shown in figure 25 for various values of n at $x/L = 0.838$. Since the experimental effective incipient Mach number for all configurations tested was close to $M_b = 0.14$, this value was used as a basis to compare the theoretical and experimental trends of amplitude shown plotted against mass flow in figures 26 and 27. The theoretical curves are drawn for $x/L = 0.838$ while the experimental points include values at $x/L = 0.838$ and $x/L = 0.919$ (gages 4 with $L/D = 14.91$ and 29.82). However, from figure 24, it may be seen that there is only a slight difference in the predicted amplitude at the two stations. Reference 6 states that for buzzing other than the very high frequency type there is a minimum of two complete wave traversals per cycle (n must be equal to or greater than 2) and the pressure records of the present tests showed most of the runs to have frequencies corresponding to values of n between 2 and 3. Consequently, only the corresponding theoretical curves are shown for n equal to 2 and 3. The general agreement for the lower amplitudes tends to substantiate the theory and the assumptions involved, while the agreement at the higher amplitudes is only a coincidence and must not be construed to mean the theory is applicable to large amplitudes.

The experimental results indicate that the supersonic diffuser configurations, when used in conjunction with the same subsonic diffuser, yield similar curves of amplitude versus mass-flow decrement. The value of M_b, however, may often depend largely on the supersonic configuration.

A simplified method for predicting the mass-flow reduction below the value at start of buzz without exceeding a given small pressure amplitude may be obtained from the linearized theory. Since n usually decreases (frequency increases) as the mass flow is reduced (see refs. 6 and 7) for a given configuration, the value of n may be assumed to be 4 or greater at the start of buzz. Higher values of n will yield lower permissible mass-flow reductions for a given amplitude. In other words, the "factor of safety" of the prediction increases as the chosen value of n increases. Then employing values of m_b and M_b assumed from geometry of the ram jet or experimentally determined, the permissible reduction in mass flow for a given small amplitude of pressure pulsation may be obtained from equations (28), (29), and (30).

CONCLUDING REMARKS

1. Cold-flow tests at a Mach number of 1.94 of ram-jet models having scale factors of 3.15:1 and Reynolds number ratios of 4.75:1 with several supersonic diffuser configurations showed only small variations in performance between geometrically similar models. The predominant variation in steady-flow performance resulted from the larger boundary layer in the combustion chamber of the low Reynolds number model. The conditions at which buzz originated were nearly the same for the same supersonic diffuser (cowling-position angle) configurations in both large and small diameter models. There was no appreciable variation in stability limits of any of the models when the combustion-chamber length was increased by a factor of three. The unsteady-flow performance and wave patterns were also similar when considered on a reduced-frequency basis depending on the relative lengths of the model. The negligible effect of Reynolds number on stability of the off-design configurations was not anticipated in view of the importance of boundary layer to stability, and this result should not be construed to be generally applicable.

2. The velocity profile in the combustion chamber at both Reynolds numbers was appreciably influenced by an angle of attack of $1/2^\circ$. The external shock pattern was noticeably affected only for the lower cowling-position angles. The pressure recovery and mass-flow values at the start of buzz were not noticeably affected.

3. From a theory developed on a quasi-one-dimensional-flow basis, it was found that the stability of the ram jet is dependent upon the instantaneous values of mass flow and total pressure recovery of the supersonic diffuser and immediate neighboring subsonic diffuser. Conditions for stable and unstable flow were presented.

4. The model assumed in the resonator analysis of Sterbentz and Evvard may be considered a rough approximation to the actual phenomena when applied for purposes of obtaining the general trends and orders of magnitude of frequency and amplitude of oscillation providing the wave length of the highest frequency component of the oscillation be much larger than the length of the ram jet. The resonator analysis is not applicable when considering the initial stability of the inlet without combustion and should not be so applied to obtain such stability criteria.

5. A simple theory for predicting the approximate amplitude of small pressure pulsation in terms of mass-flow decrement from minimum-stable mass flow was developed and found to agree with experiments.

Langley Aeronautical Laboratory,
National Advisory Committee for Aeronautics,
Langley Field, Va., July 28, 1953.

REFERENCES

1. Oswatitsch, Kl.: Der Druckrückgewinn bei Geschossen mit Rückstossantrieb bei hohen Überschallgeschwindigkeiten (Der Wirkungsgrad von Stossdiffusoren). Bericht Nr. 1005, Forsch. und Entwickl. des Heereswaffenamtes (Göttingen), 1944. (Available in English translation as NACA TM 1140.)

2. Comenzo, Raymond J., and Mackley, Ernest A.: Preliminary Investigation of a Rectangular Supersonic Scoop Inlet With Swept Sides Designed For Low Drag at a Mach Number of 2.7. NACA RM L52J02, 1952.

3. Hunczak, Henry R., and Kremzier, Emil J.: Characteristics of Perforated Diffusers at Free-Stream Mach Number 1.90. NACA RM E50B02, 1950.

4. Connors, James F.: Effect of Ram-Jet Pressure Pulsations on Supersonic-Diffuser Performance. NACA RM E50H22, 1950.

5. Ferri, Antonio, and Nucci, Louis M.: The Origin of Aerodynamic Instability of Supersonic Inlets at Subcritical Conditions. NACA RM L50K30, 1951.

6. Trimpi, Robert L.: An Analysis of Buzzing in Supersonic Ram Jets by a Modified One-Dimensional Nonstationary Wave Theory. NACA RM L52A18, 1952.

7. Sterbentz, William H., and Evvard, John C.: Criterions for Prediction and Control of Ram-Jet Flow Pulsations. NACA RM E51C27, 1951.

8. Orlin, W. J., and Dunsworth, L. C.: A Criterion for Flow Instability in Supersonic Diffuser Inlets. Rep. No. 5144 (Contracts Noa(s)9403 and AF 33(038)-11231) Marquardt Aircraft Co., Apr. 2, 1951.

9. Sterbentz, William H., and Davids, Joseph: Amplitude of Supersonic Diffuser Flow Pulsations. NACA RM E52I24, 1952.

10. Connors, James F., and Schroeder, Albert H.: Experimental Investigation of Pressure Fluctuations in 3.6-Inch Ram Jet at Mach Number 1.92. NACA RM E9H12, 1949.

11. Kraushaar, Robert J.: Manometers in Pulsating Systems. Tech. Memo. NYU-14, U. S. N. and U. S. Air Force Project SQUID, New York Univ., Aug. 22, 1951.

TABLE I.- ORDINATES OF MODELS

*Axial location, x/D	Radii of 4.026-inch-diameter model		Radii of 1.278-inch-diameter model	
	Center body	Inner cowling	Center body	Inner cowling
	r_1/R_o	r_2/R_o	r_1'/R_o'	r_2'/R_o'
-0.3095	0	-----	0	-----
0	0.290	0.601	0.294	0.599
.02	.308	.611	.313	.608
.04	.327	.622	.332	.617
.06	.345	.631	.350	.626
.08	.362	.639	.369	.634
.10	.377	.647	.386	.643
.11	.383	.650	.391	.647
.12	.389	.653	.395	.651
.13	.394	.656	.397	.655
.14	.397	.660	.400	.658
.15	.398	.662	.399	.661
.16	.398	.665	.399	.664
.18	.398	.669	.398	.670
.20	.397	.673		.675
.25	.396	.681		.684
.30	.395	.686		.688
.40	.393	.693		
.50	.391	.700		
.75	.385	.716		
1.00	.379	.732		
1.50	.368	.765		
2.00	.356	.798		
2.50	.345	.830		
3.00	.333	.863		
3.44	.324	.892		
3.50	.324	.896		
3.55	.324	.899		
3.65	.319	.905	Same as 4.026 model	Same as 4.026 model
3.82	.308	.916		
4.00	.297	.929		
4.50	.268	.961		
5.00	.239	.994		
5.10	.233	1.0		
5.50	.209			
6.00	.180			
6.15	.171			
6.32	.162			
6.50	.151			
6.97	.124			
7.00	.124			
7.20	.099			
7.30	.079			
7.40	.037			
7.47	0	1.0		
To valve	Values remain constant for remainder of models			

*Note: $\frac{x}{D} = 0$ is taken at cowling lip

NACA

TABLE II.- RAKE ORDINATES IN VERTICAL PLANE

Rake tube number	Ordinate = Radius rake / Radius duct	
	Large model	Small model
1, 9	0.910	0.889
2, 8	.694	.702
3, 7	.468	.468
4, 6	.231	.234
5	0	0

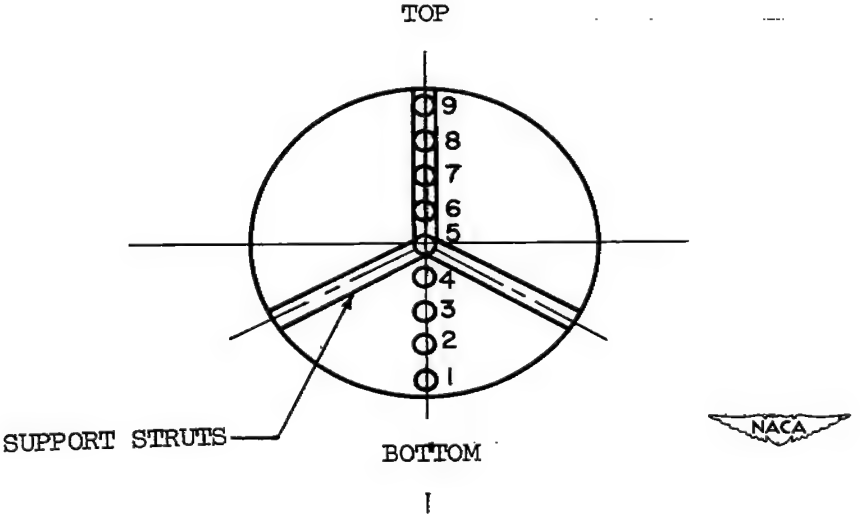

TABLE III.- VALUES OF PARAMETERS AT START OF BUZZ

Configuration	Mass-flow ratio	Pressure recovery	Static/Tank pressure ratio		Valve position
			Gage 1	Gage 4	
1.278 - 14.91 - 48.1°	0.91	0.795	0.744	0.782	1.35
1.278 - 29.82 - 48.1°	.925	.790	.738	.778	1.345
4.026 - 14.91 - 48.1°	.955	.795	.727	.781	2.12
4.026 - 29.82 - 48.1°	.945	.790	.733	.782	2.12
1.278 - 14.91 - 44.2°	.98	.844	.805	.837	1.34
1.278 - 29.82 - 44.2°	.98	.844	.804	.835	1.34
4.026 - 14.91 - 44.2°	.98	.848	.804	.842	2.07
4.026 - 29.82 - 44.2°	.98	.844	.802	.838	2.06
1.278 - 14.91 - 40.1°	.85	.846	.817	.840	1.31
1.278 - 29.82 - 40.1°	.85	.846	.814	.844	1.31
4.026 - 14.91 - 40.1°	.86	.832	.806	.825	1.965
4.026 - 29.82 - 40.1°	.86	.832	.804	.829	1.96

NACA

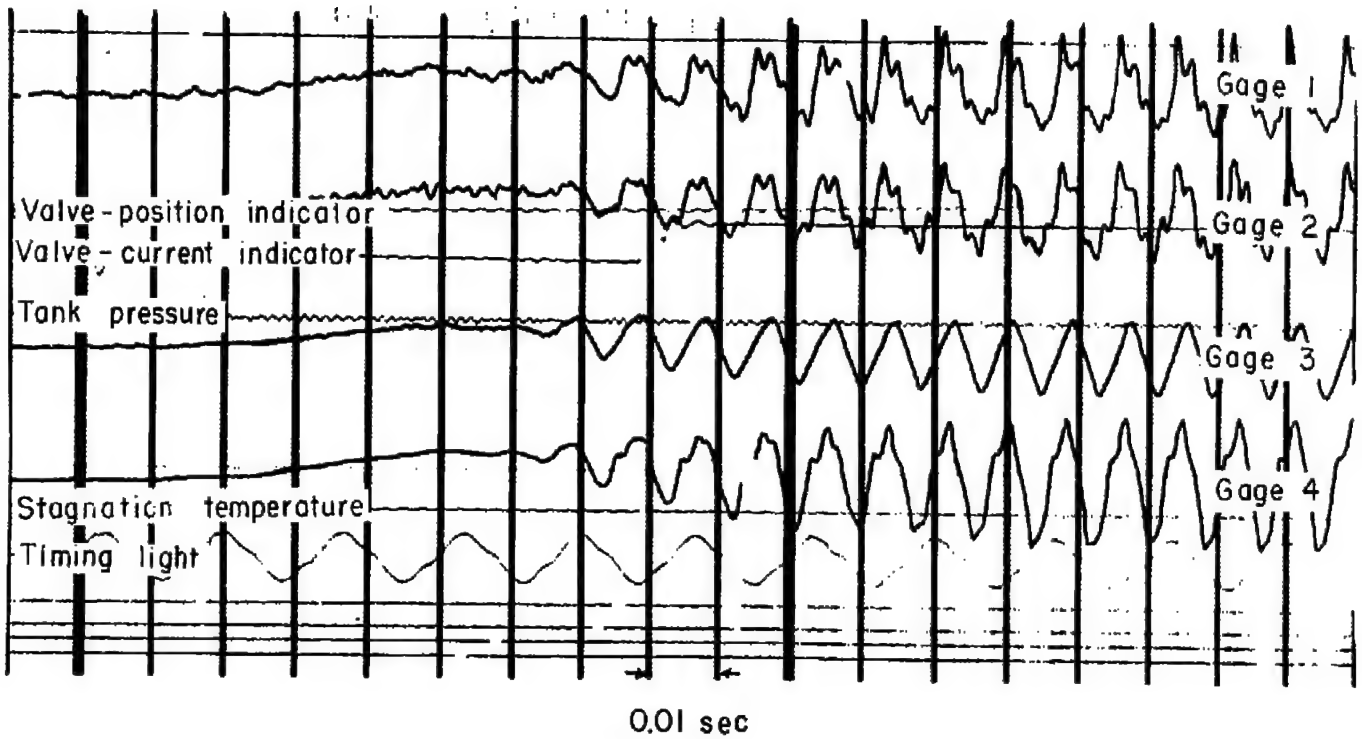

Figure 1.- Typical pressure record of start of buzz for configuration 1.278 - 14.91 - 44.2°. Time is increasing to right and pressure is positive upward.

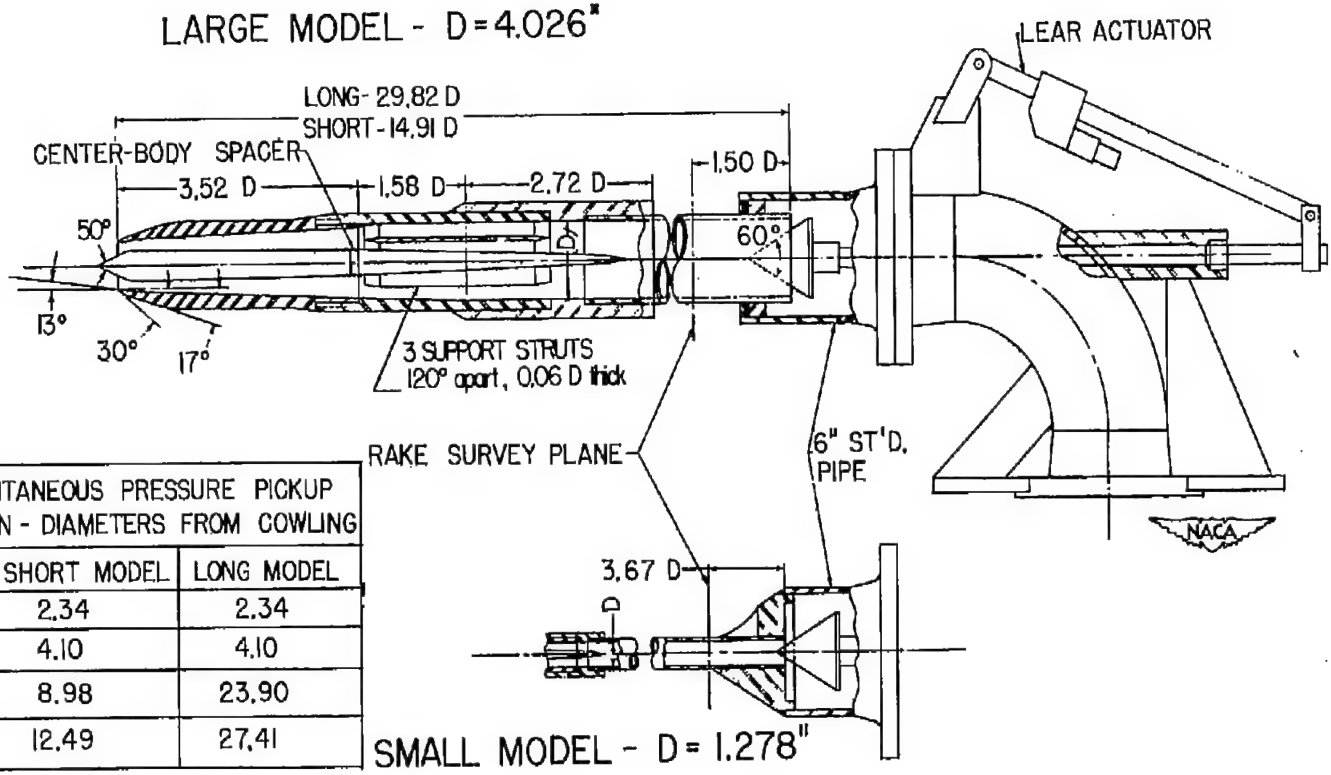

INSTANTANEOUS PRESSURE PICKUP LOCATION - DIAMETERS FROM COWLING		
GAGE	SHORT MODEL	LONG MODEL
1	2.34	2.34
2	4.10	4.10
3	8.98	23.90
4	12.49	27.41

Figure 2.- Schematic diagram of models tested. Small model is similar to large model except for transition section at plug valve.

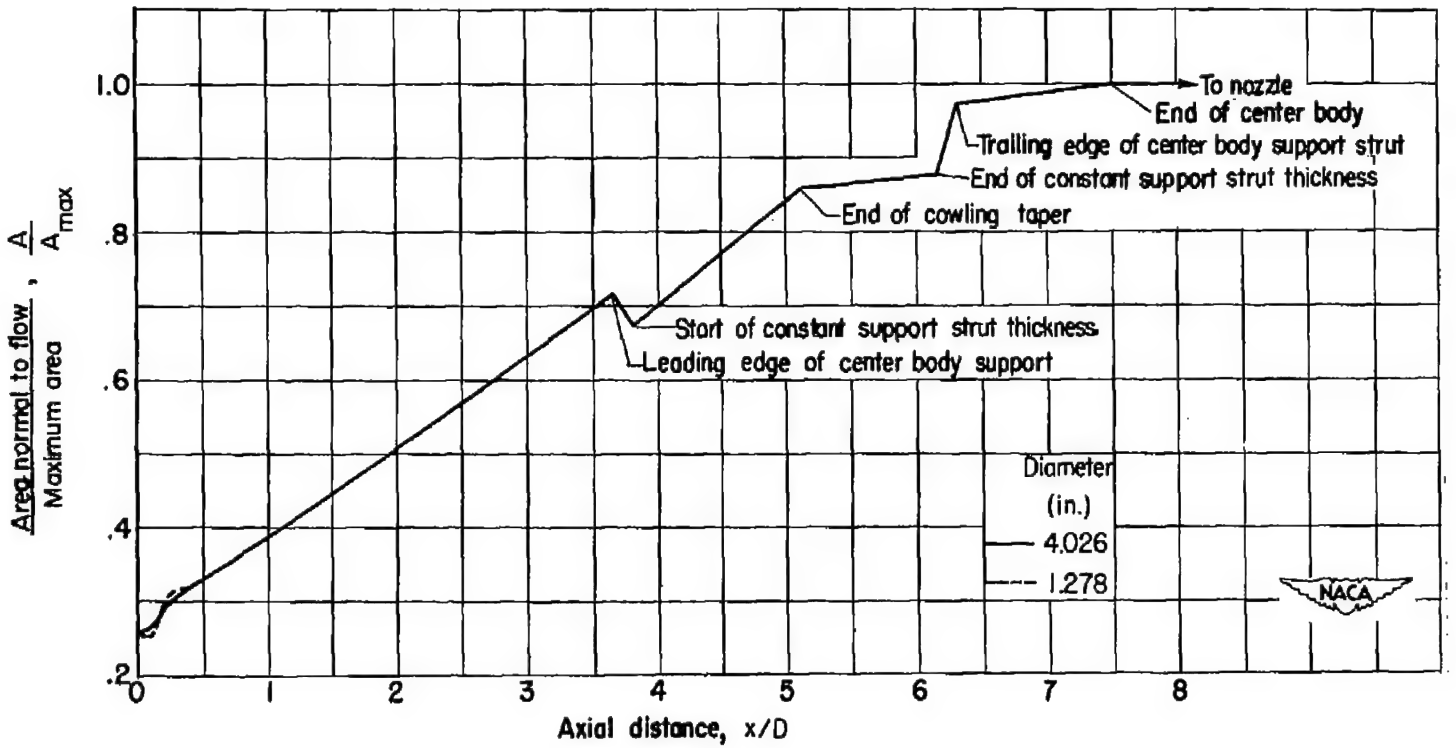

Figure 3.- Local flow area plotted against axial distance from cowling for models tested. Cowling position angle 44.2°.

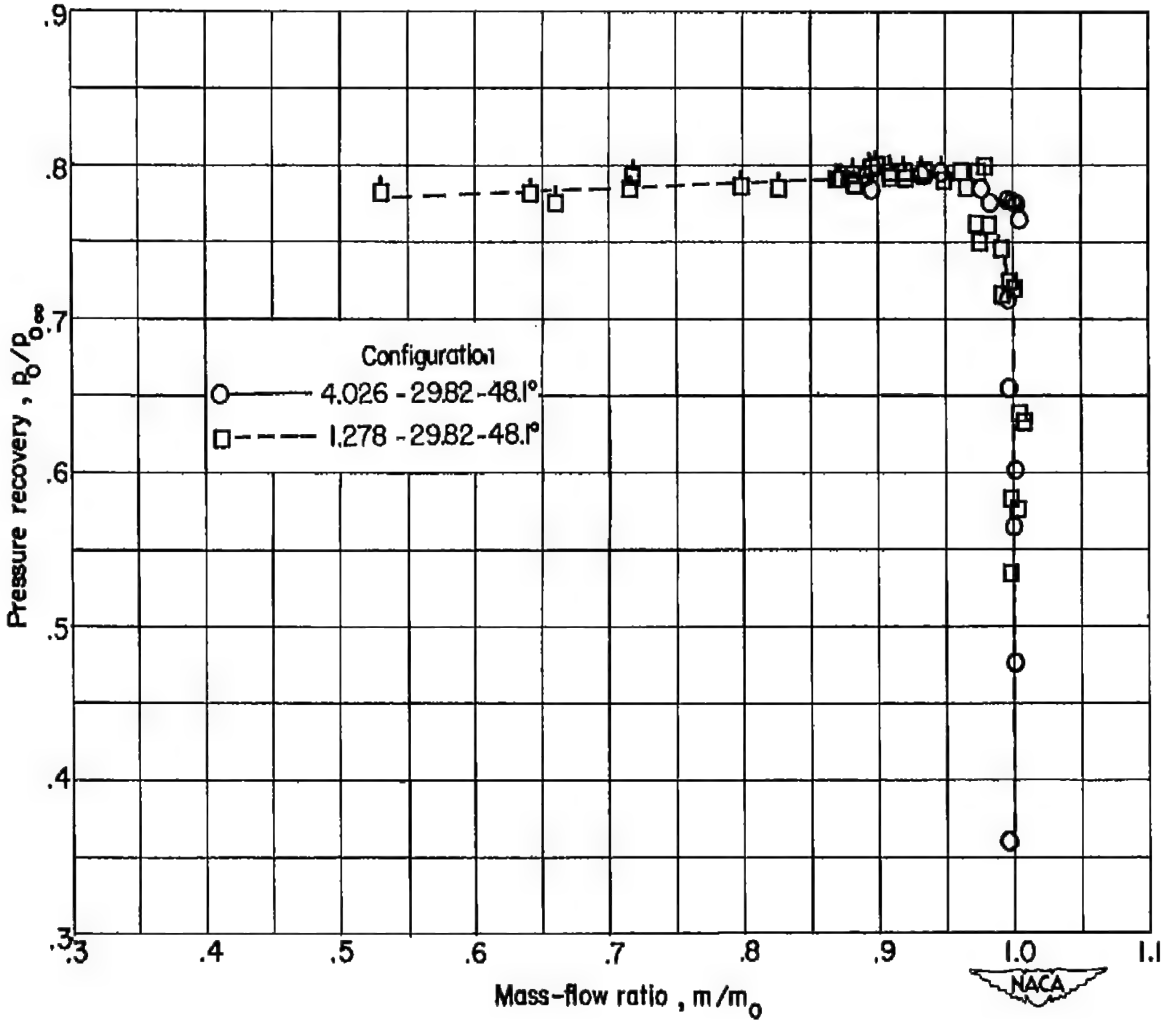

Figure 4.- Curves of pressure recovery plotted against mass-flow ratio for configurations 29.82 - 48.1°. Flagged symbols denote unsteady flow.

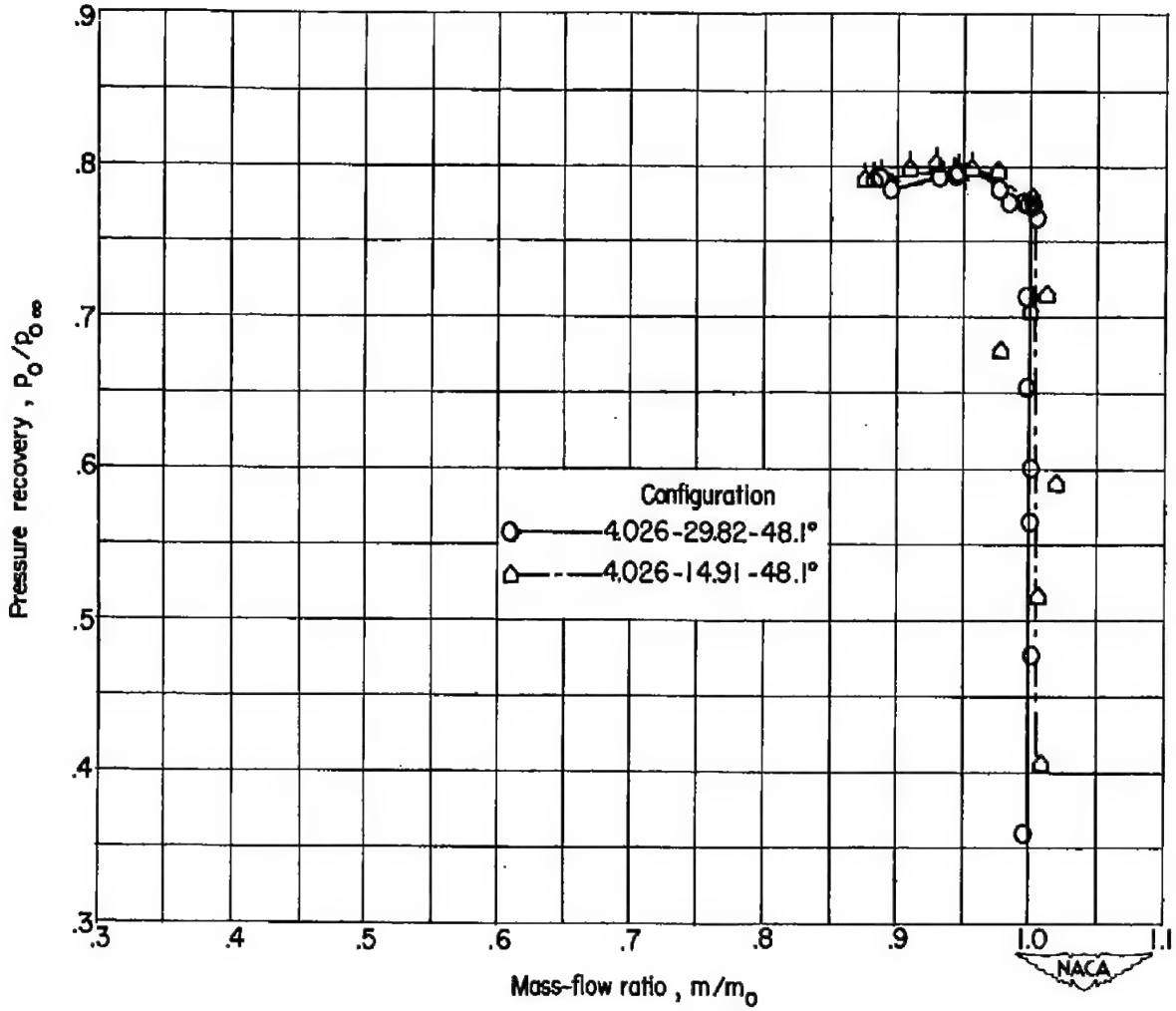

Figure 5.- Curves of pressure recovery plotted against mass-flow ratio for configurations 4.026 - 48.1°. Flagged symbols denote unsteady flow.

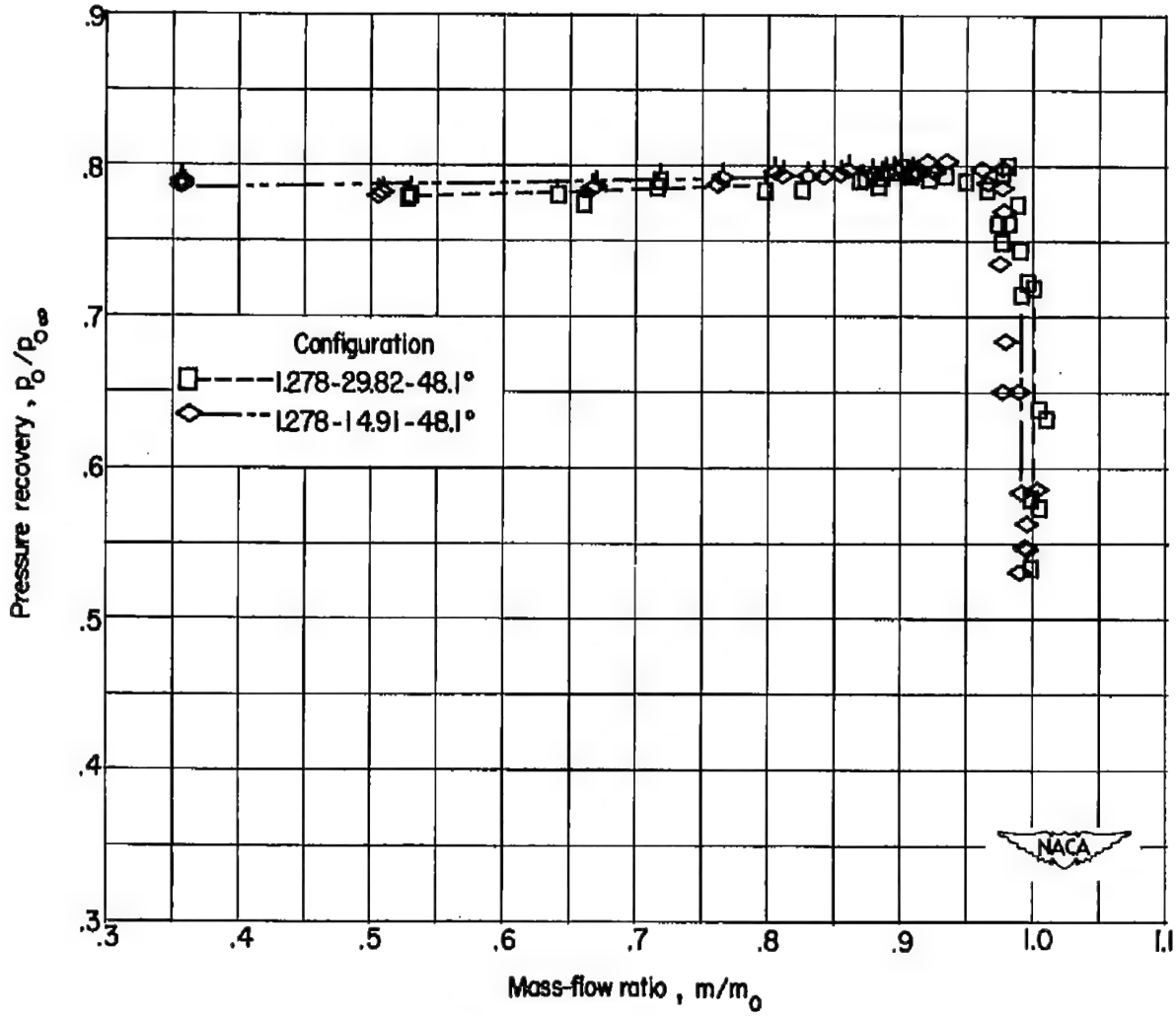

Figure 6.- Curves of pressure recovery plotted against mass-flow ratio for configurations 1.278 - 48.1°. Flagged symbols denote unsteady flow.

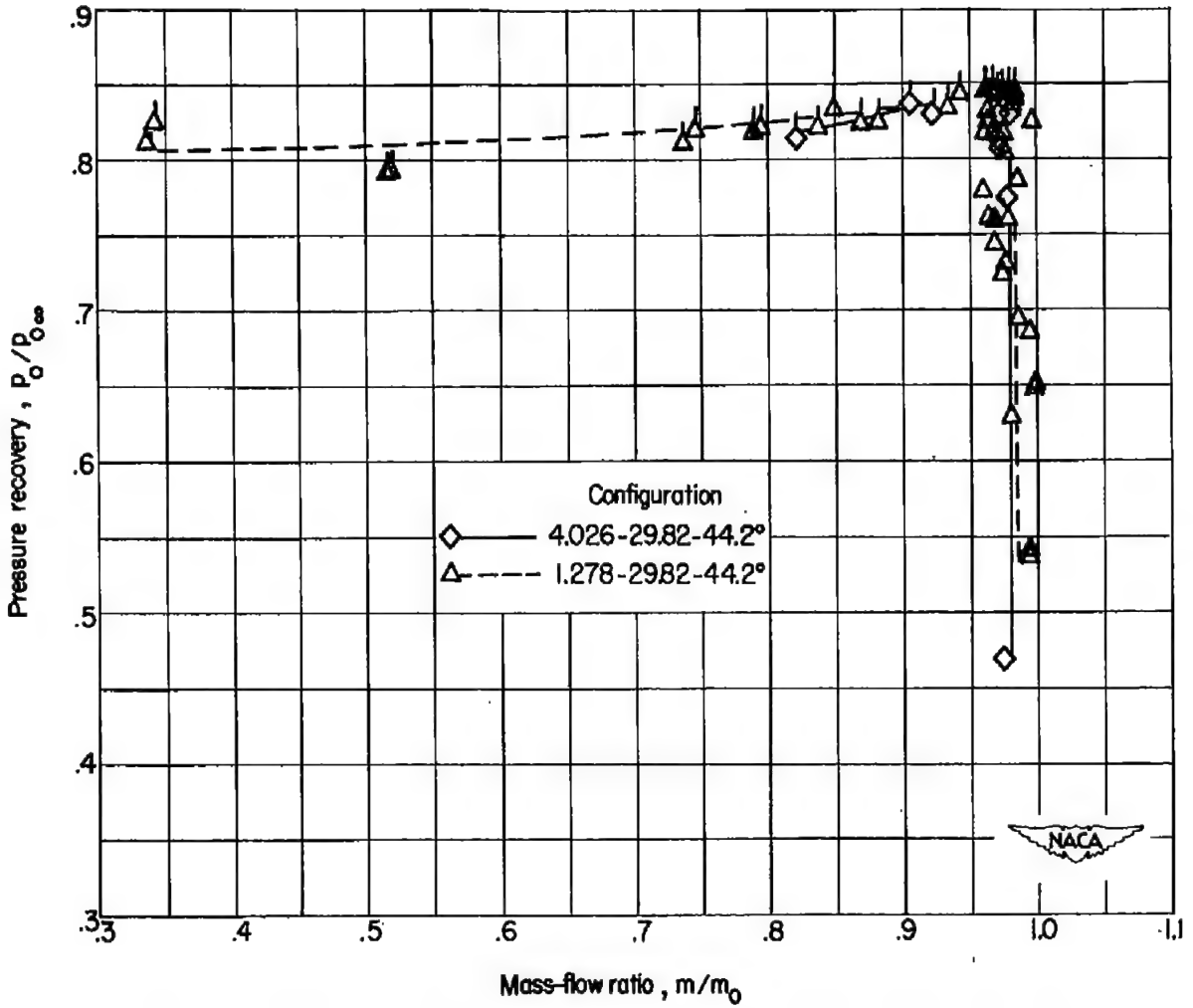

Figure 7.- Curves of pressure recovery plotted against mass-flow ratio for configurations 29.82 - 44.2°. Flagged symbols denote unsteady flow.

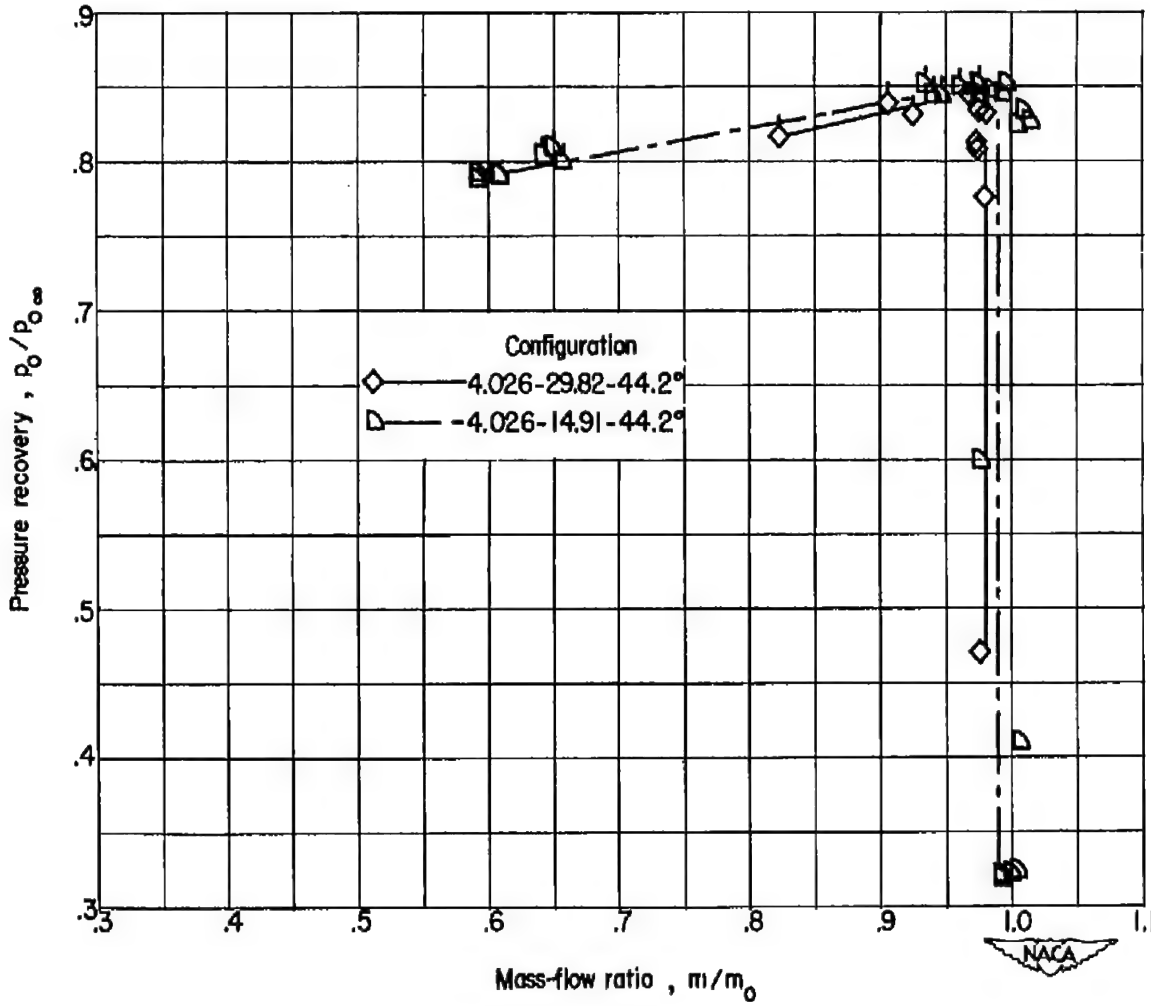

Figure 8.- Curves of pressure recovery plotted against mass-flow ratio for configurations 4.026 - 44.2°. Flagged symbols denote unsteady flow.

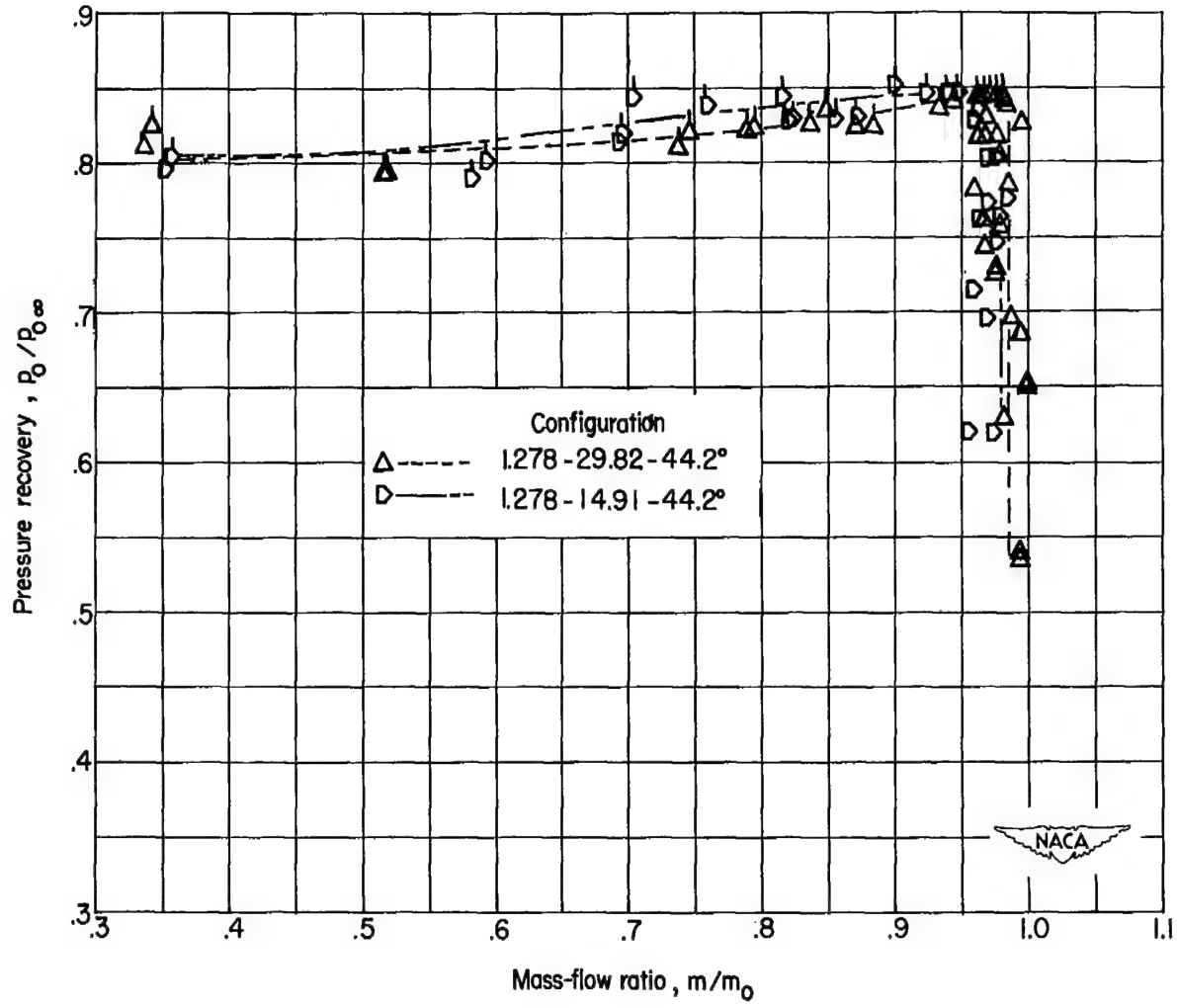

Figure 9.- Curves of pressure recovery plotted against mass-flow ratio for configurations 1.278 - 44.2°. Flagged symbols denote unsteady flow.

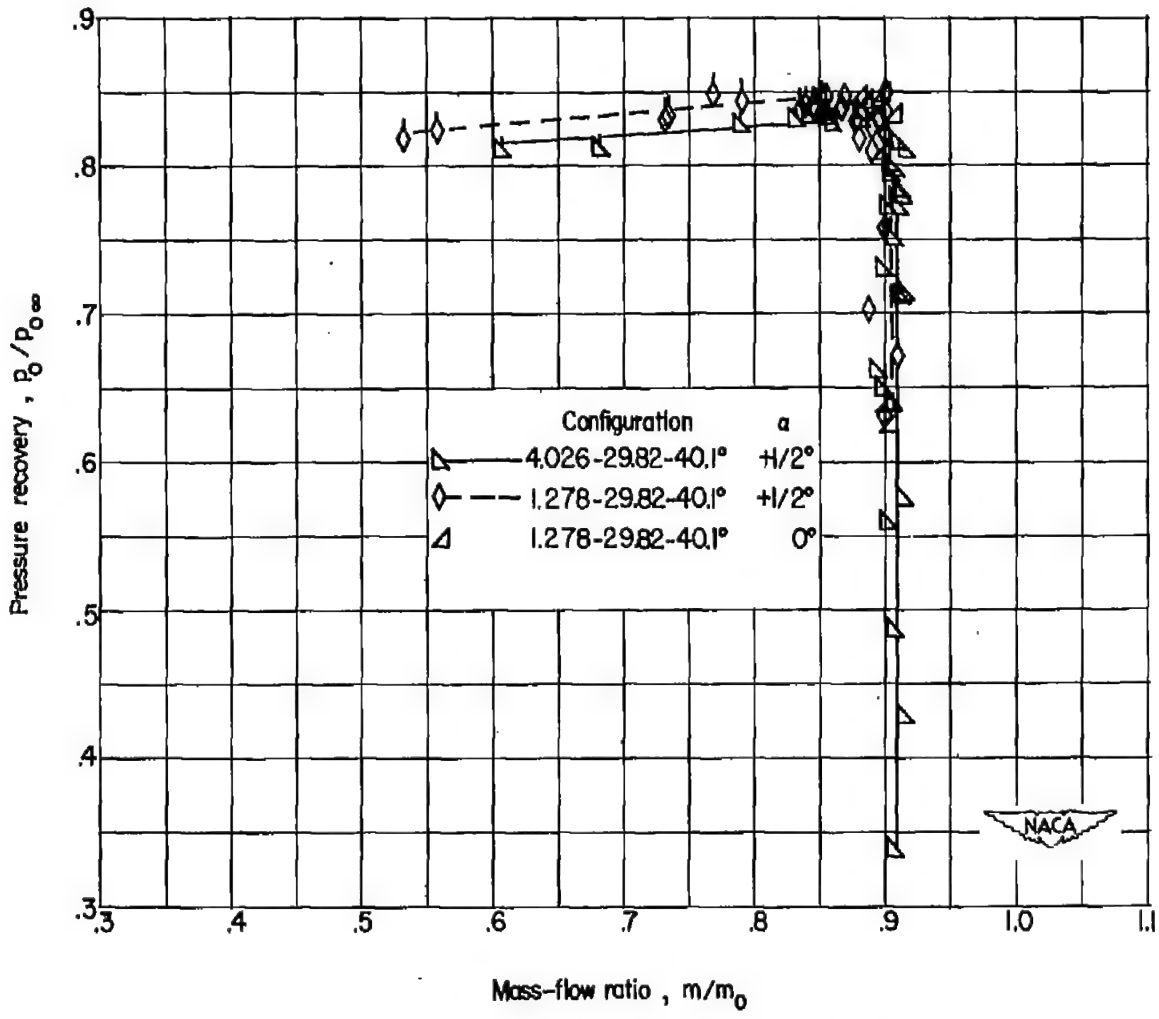

Figure 10.- Curves of pressure recovery plotted against mass-flow ratio for configurations 29.82 - 40.1°. Flagged symbols denote unsteady flow.

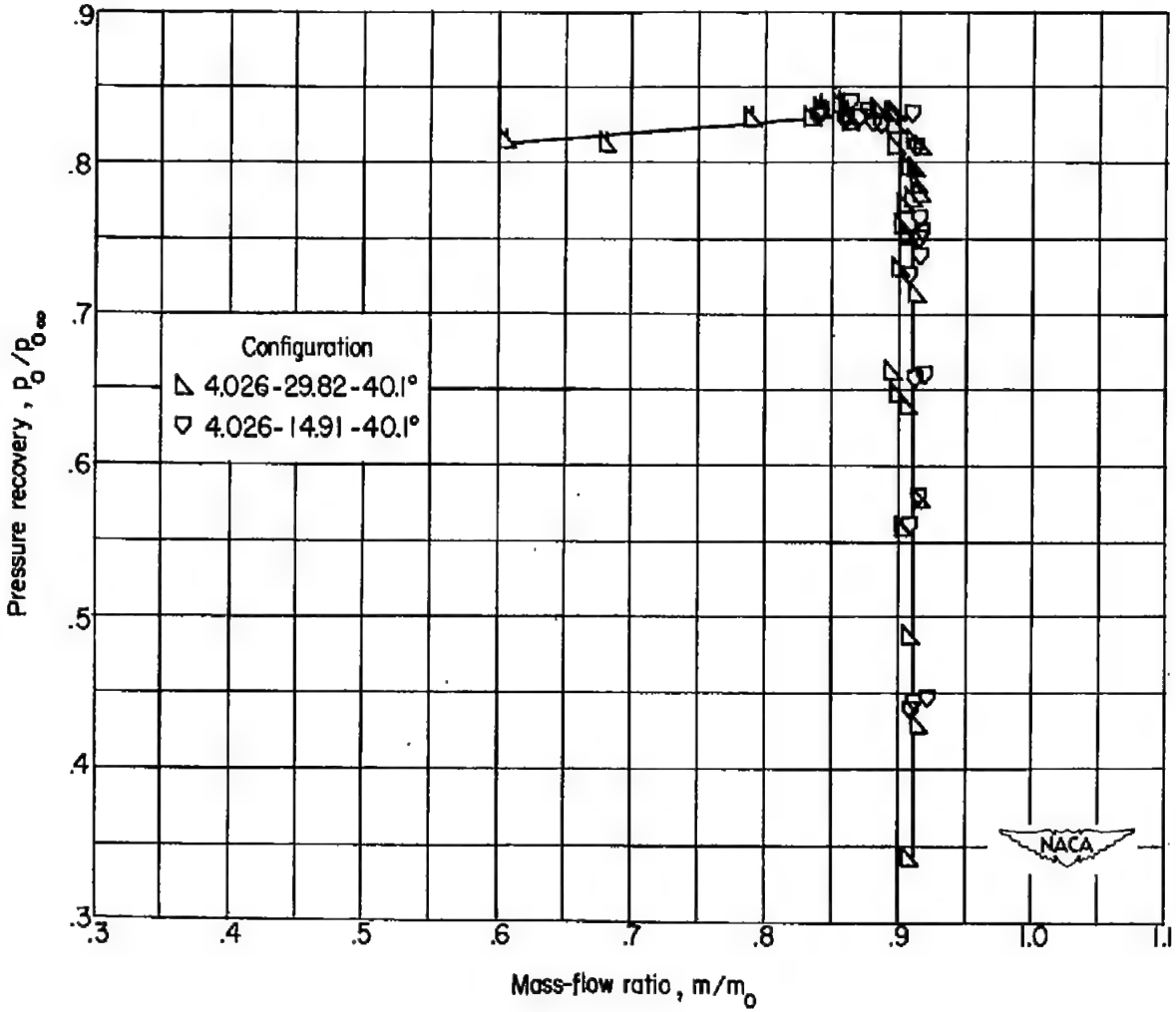

Figure 11.- Curves of pressure recovery plotted against mass-flow ratio for configurations 4.026 - 40.1°. Flagged symbols denote unsteady flow.

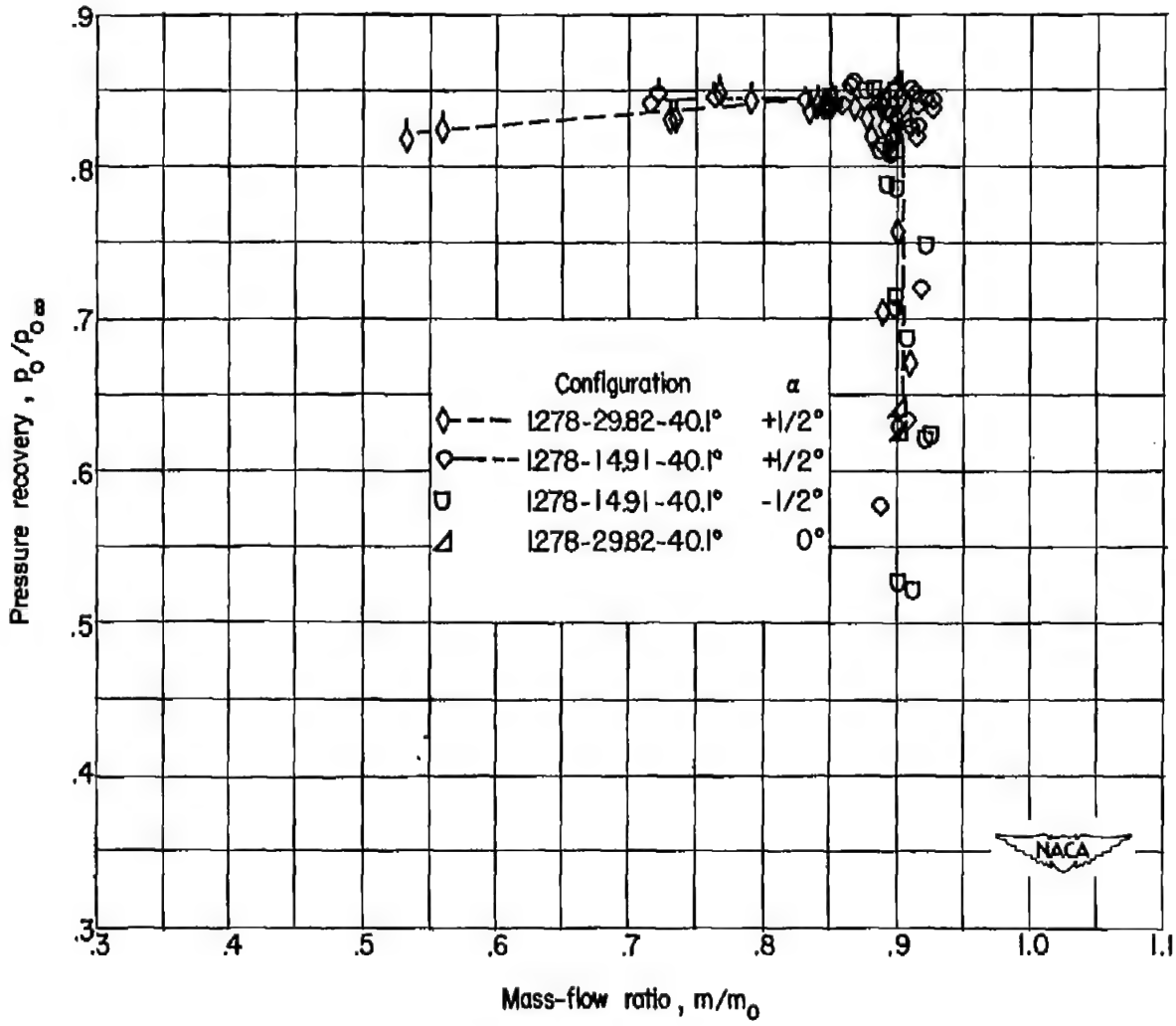

Figure 12.- Curves of pressure recovery plotted against mass-flow ratio for configurations 1.278 - 40.1°. Flagged symbols denote unsteady flow.

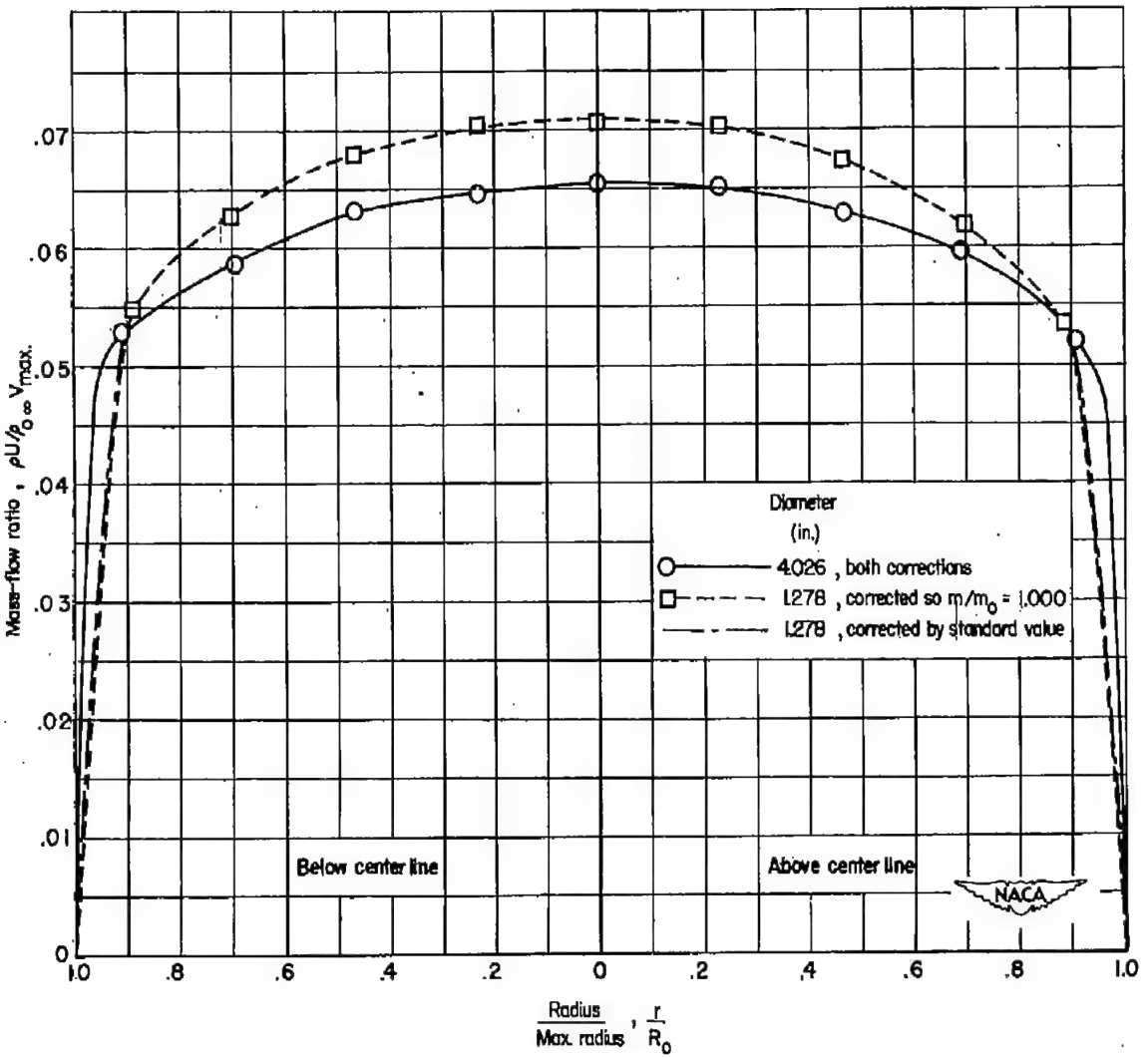

Figure 13.- Mass-flow profiles at rake survey station for configurations 29.8° - 48.1°.

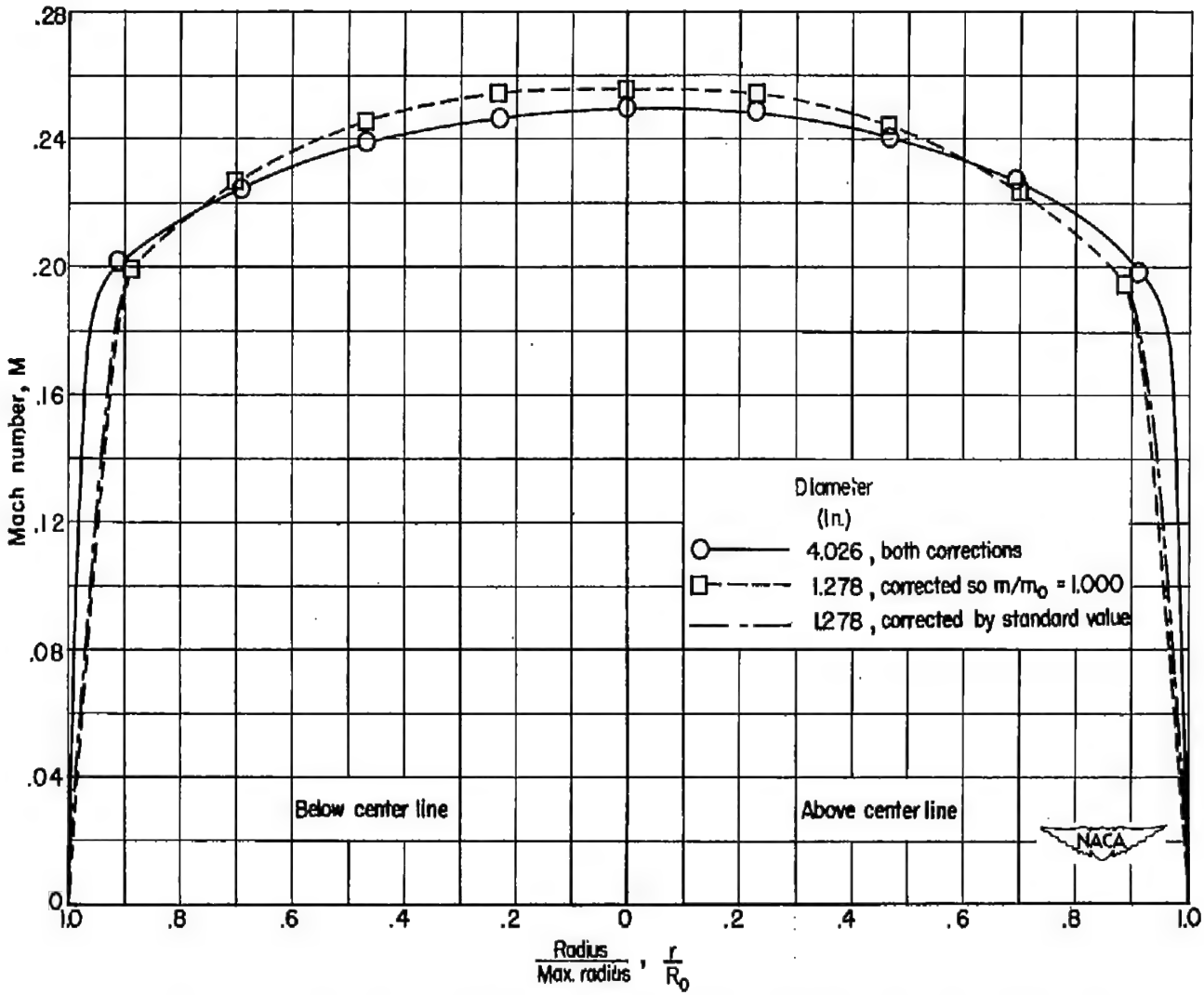

Figure 14.- Mach number profiles at rake survey station for configurations 29.82 - 48.1°.

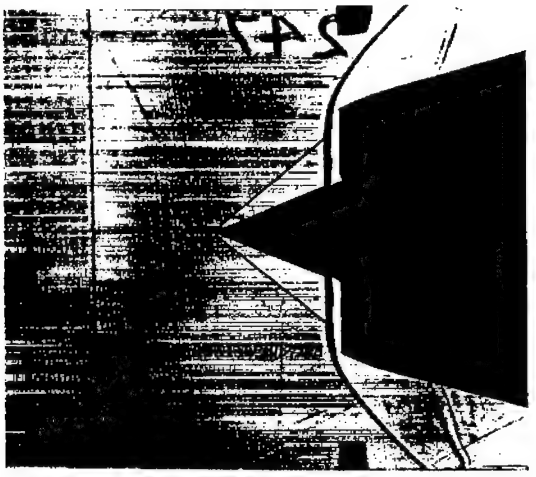

(a) Configuration 4.026-29.82-48.1°; α = +1/2°

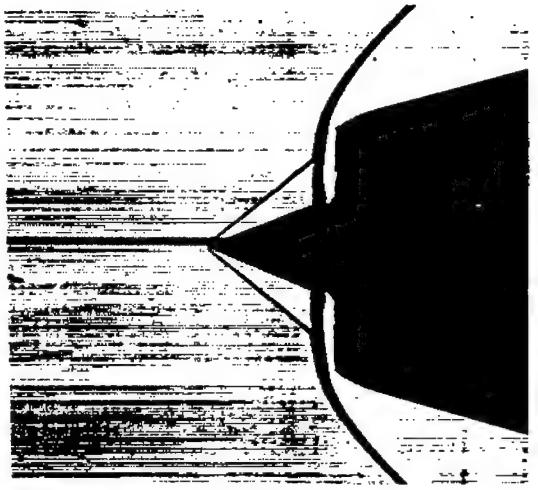

(b) Configuration 1.278-29.82-48.1°; α = +1/2°

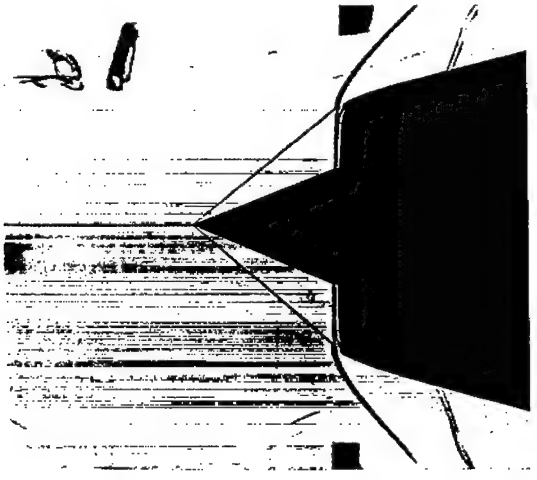

(c) Configuration 4.026-29.82-44.2°; α = +1/2°

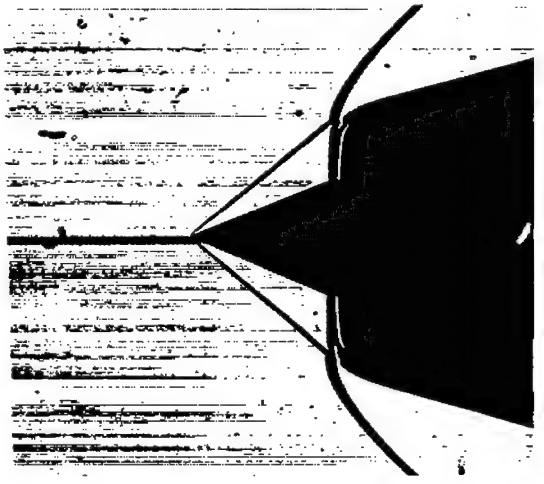

(d) Configuration 1.278-29.82-44.2°; α = +1/2°

L-80248

Figure 15.- Instantaneous spark shadowgraphs of flow patterns for minimum stable mass flow.

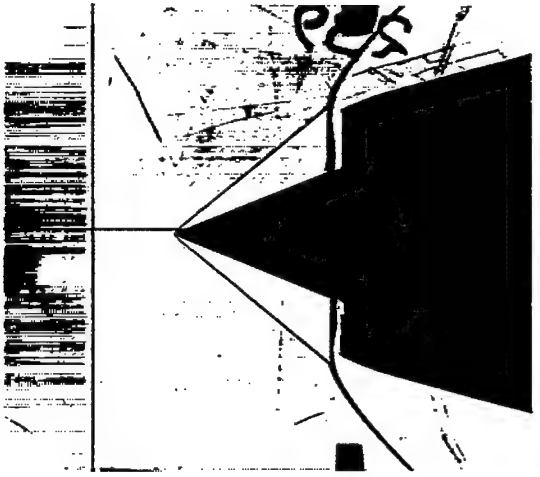

(e) Configuration 4.026-29.82-40.1°; α = +1/2°

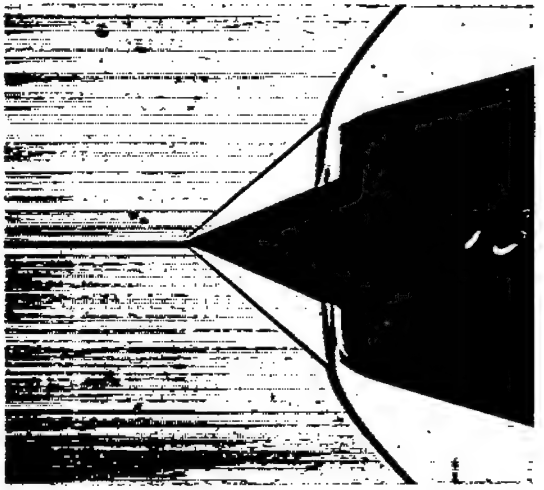

(f) Configuration 1.278-29.82-40.1°; α = +1/2°

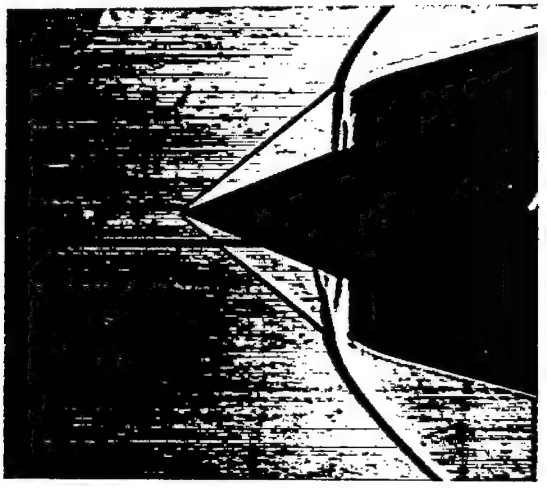

(g) Configuration 1.278-14.91-40.1°; α = −1/2°

L-80249

Figure 15.- Concluded.

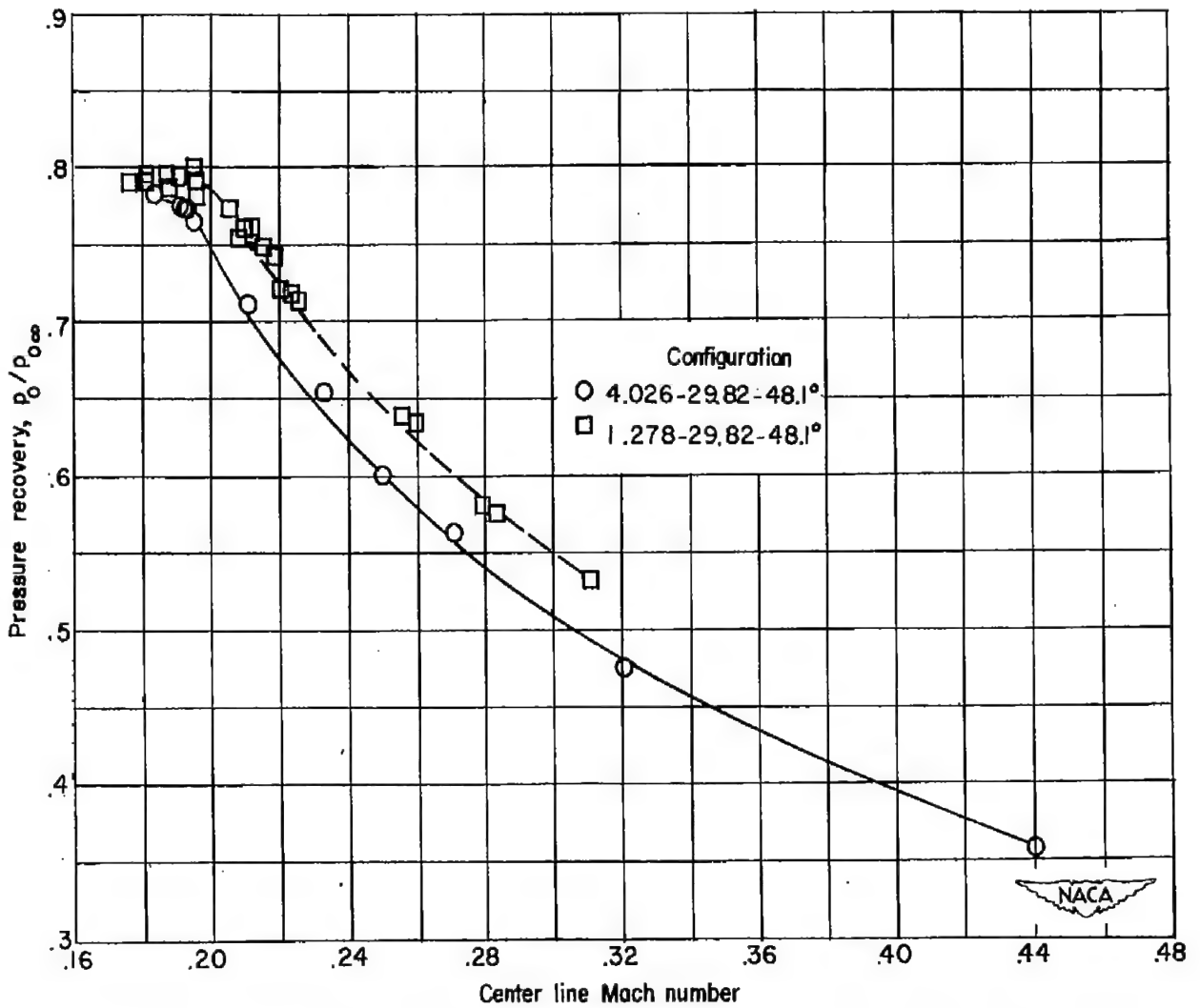

Figure 16.- Curves of average pressure recovery plotted against Mach number at center of rake survey station for configurations 29.82 - 48.1°.

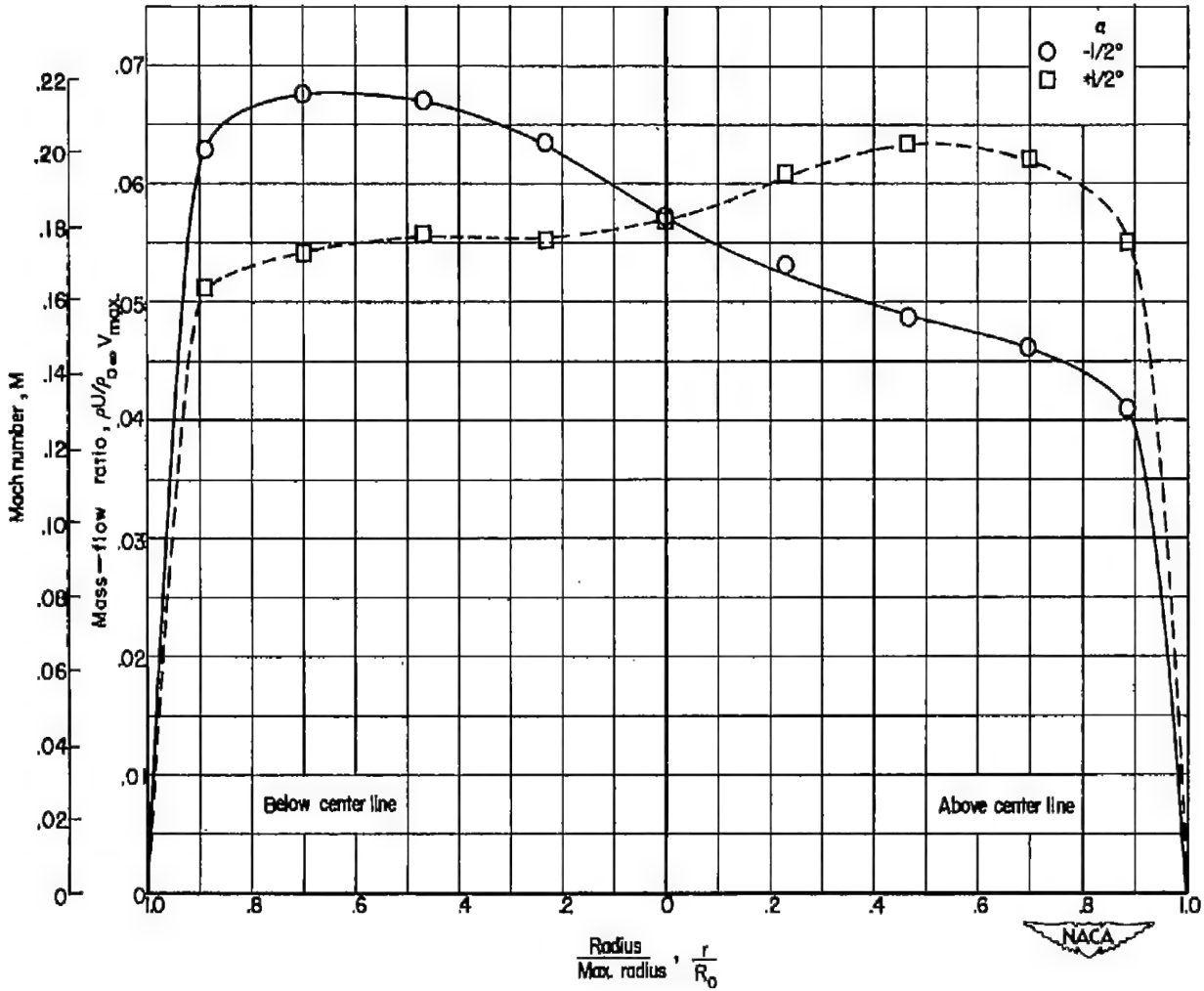

Figure 17.- Mass-flow and Mach number profiles at rake survey station for configuration 1.278 - 14.91 - 40.1° at angles of attack of $\pm\frac{1}{2}^{\circ}$.

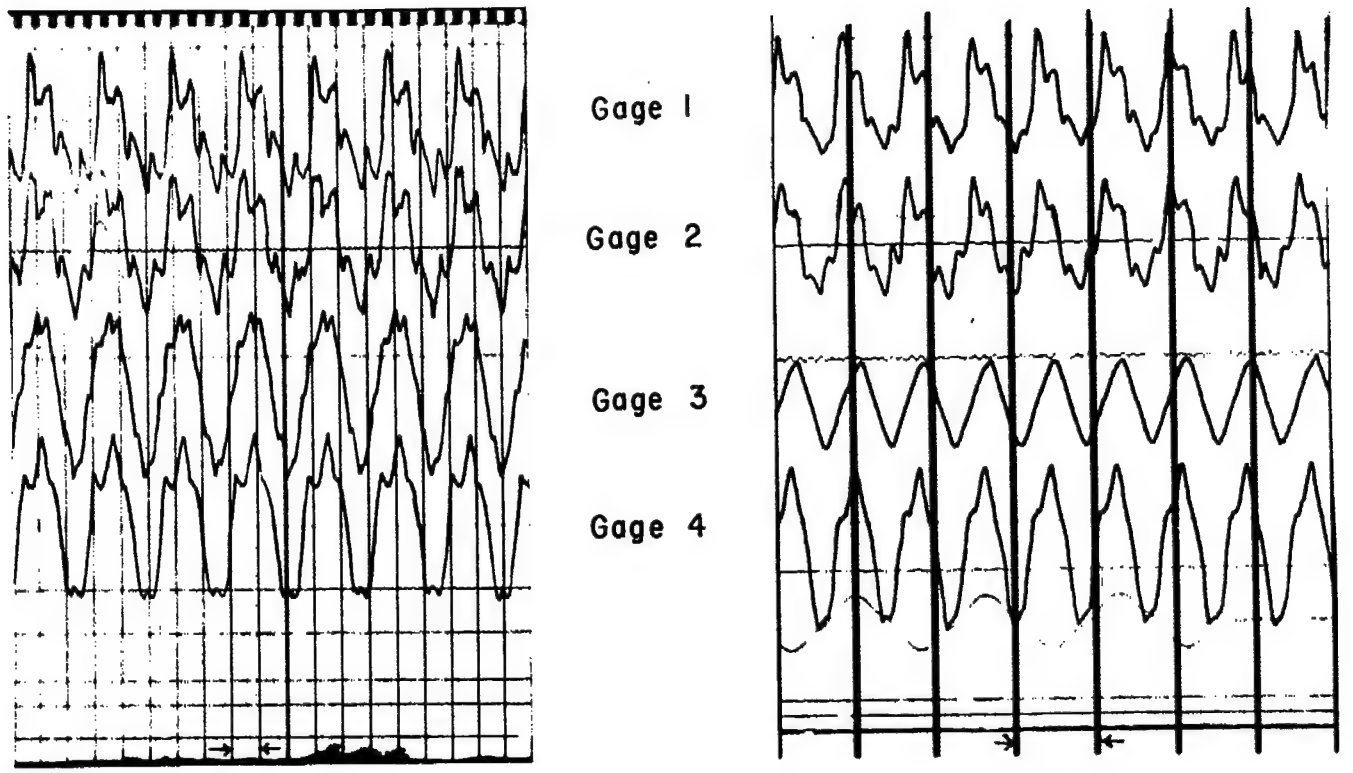

(a) Configuration 4.026 - 14.91 - 44.2°.

(b) Configuration 1.278 - 14.91 - 44.2°.

Figure 18.- Pressure-time records showing similar regular pulses in buzzing of similar configurations. Pressure is positive upward.

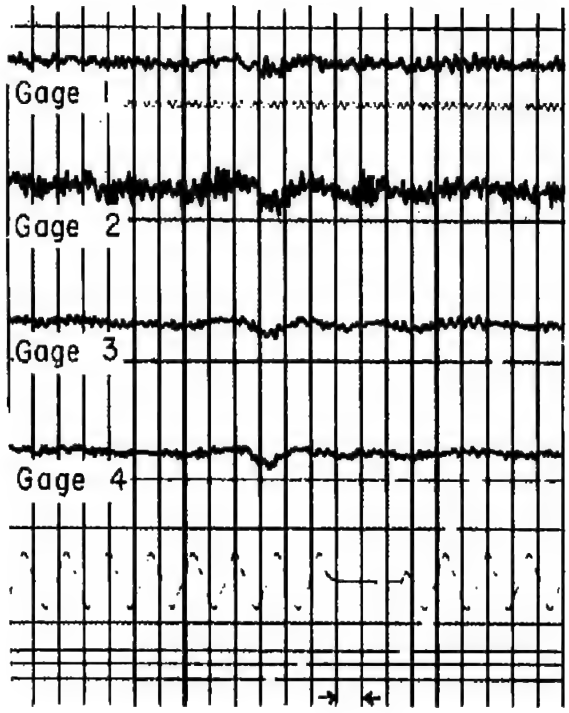

(a) Configuration 4.026 - 14.91 - 40.1°.

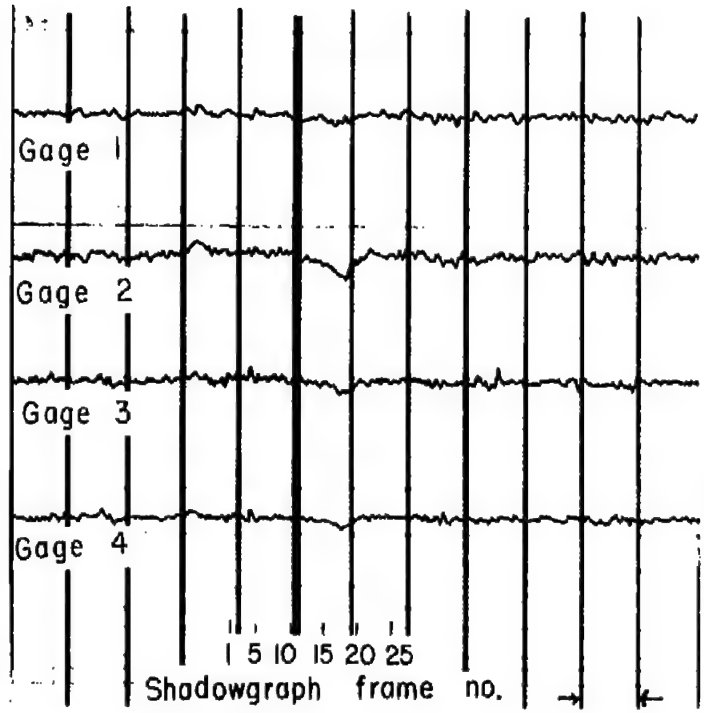

(b) Configuration 1.278 - 14.91 - 40.1°

Figure 19.- Pressure-time records showing similar isolated spasmodic pulse in buzzing of similar configurations. Pressure is positive upward.

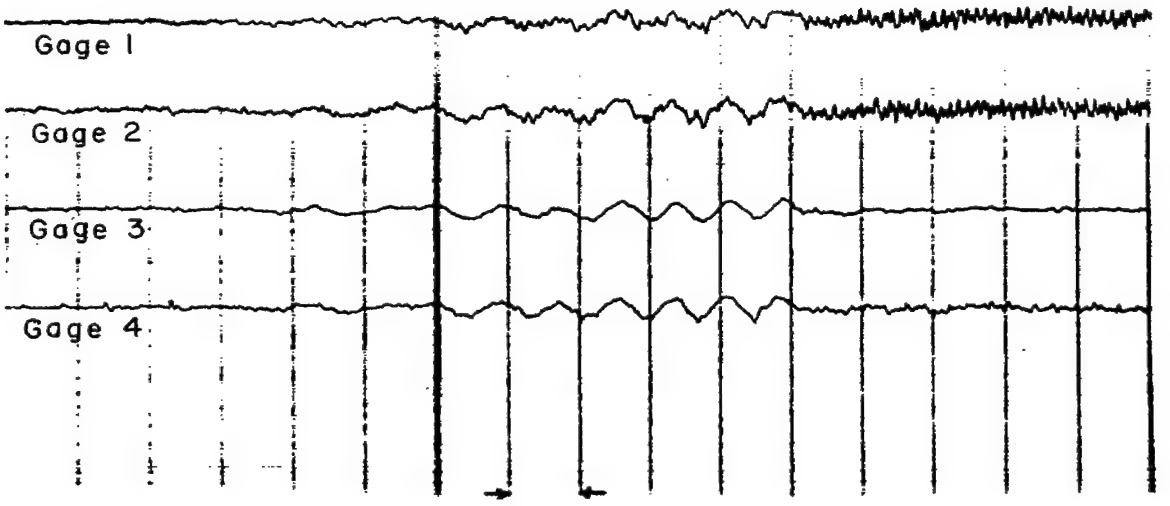

(a) Slight valve motion.

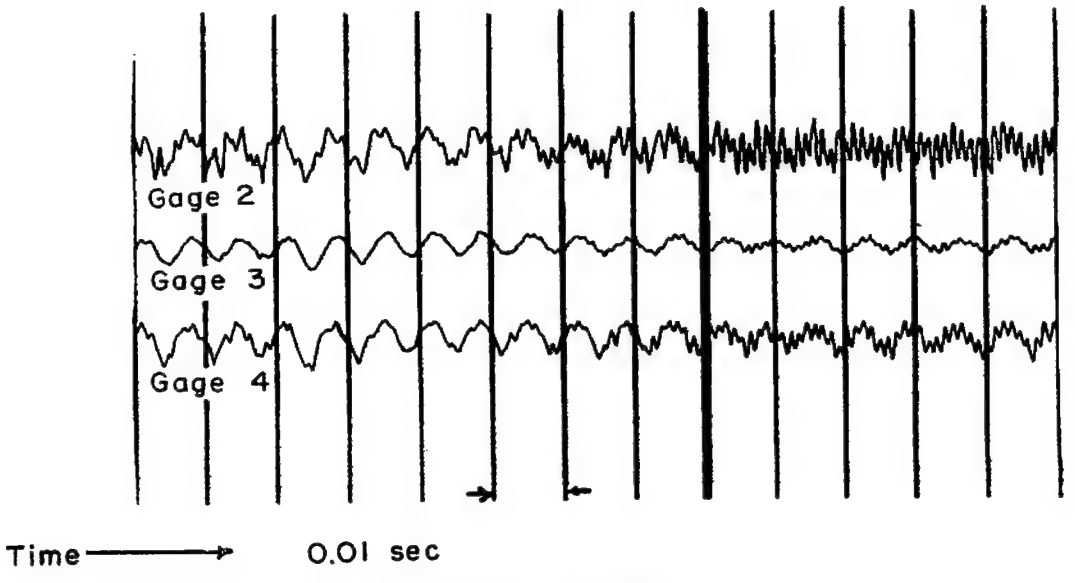

(b) No valve motion.

Figure 20.- Pressure-time records showing transition from low-frequency to high-frequency buzzing in configuration 1.278 - 14.91 - 40.1°.

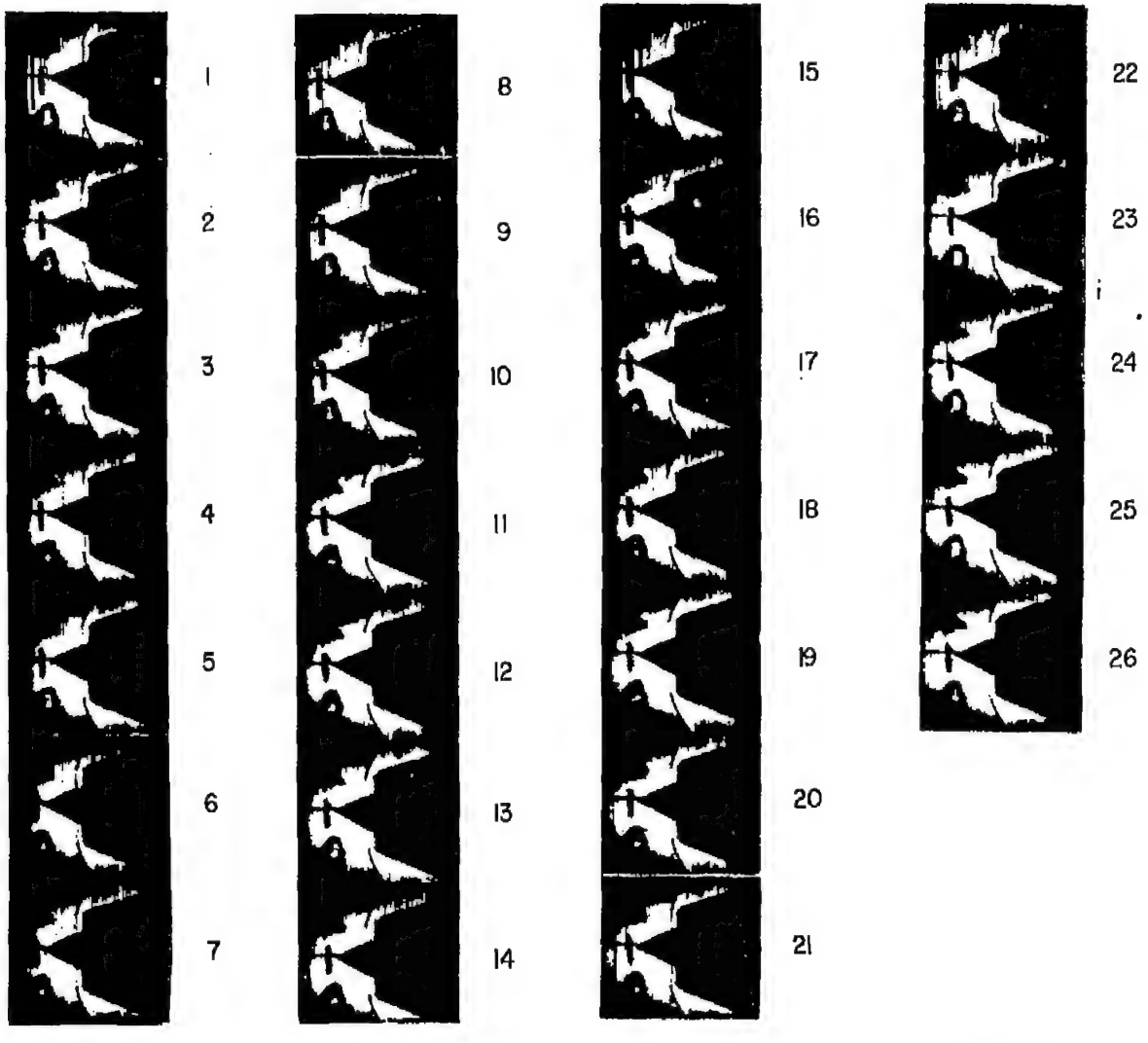

L-80250

Figure 21.- High-speed motion-picture shadowgraphs of isolated spasmodic pulse in buzzing of configuration 1.278 - 14.91 - 40.1°.

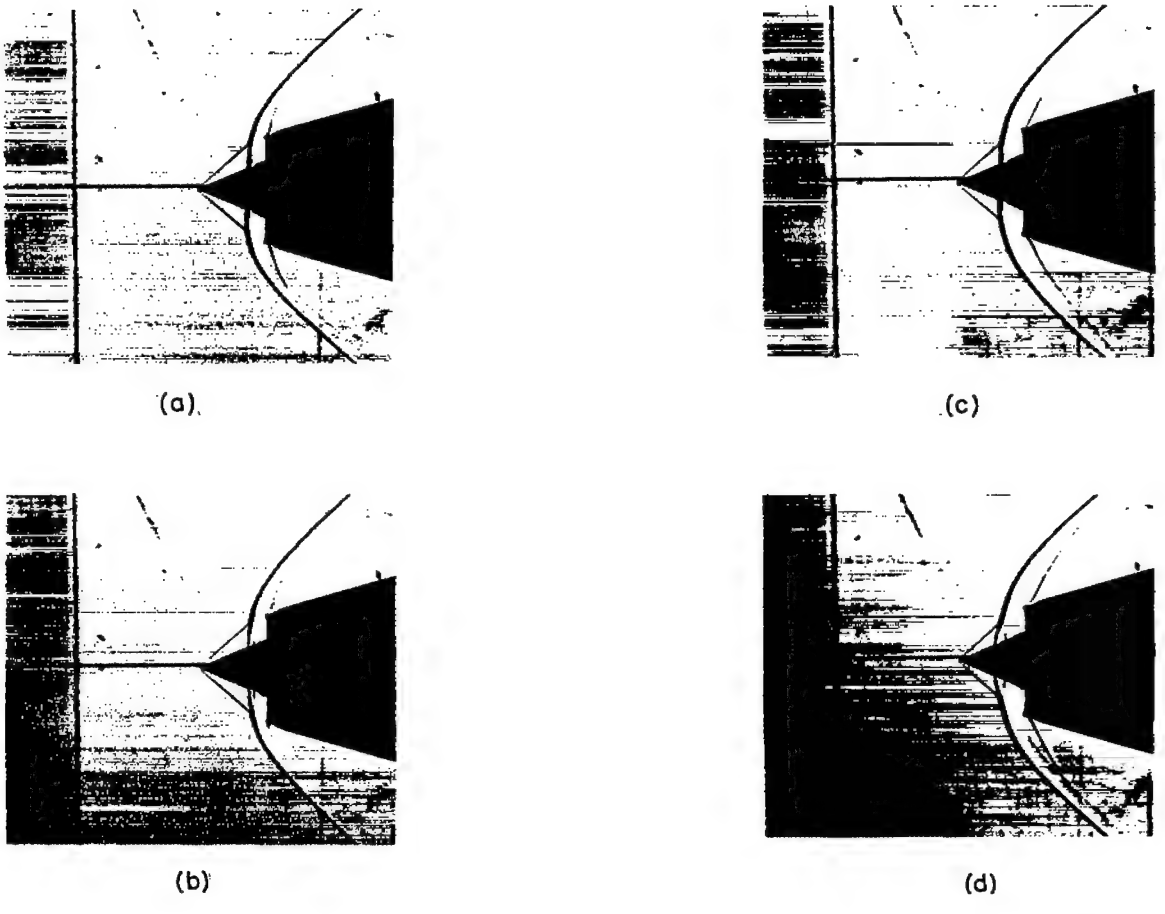

L-80251

Figure 22.- Instantaneous shadowgraphs taken during buzzing of configuration 1.278 - 14.91 - 40.1° to show variation in flow pattern at foot of shock when outer part of shock is at same position.

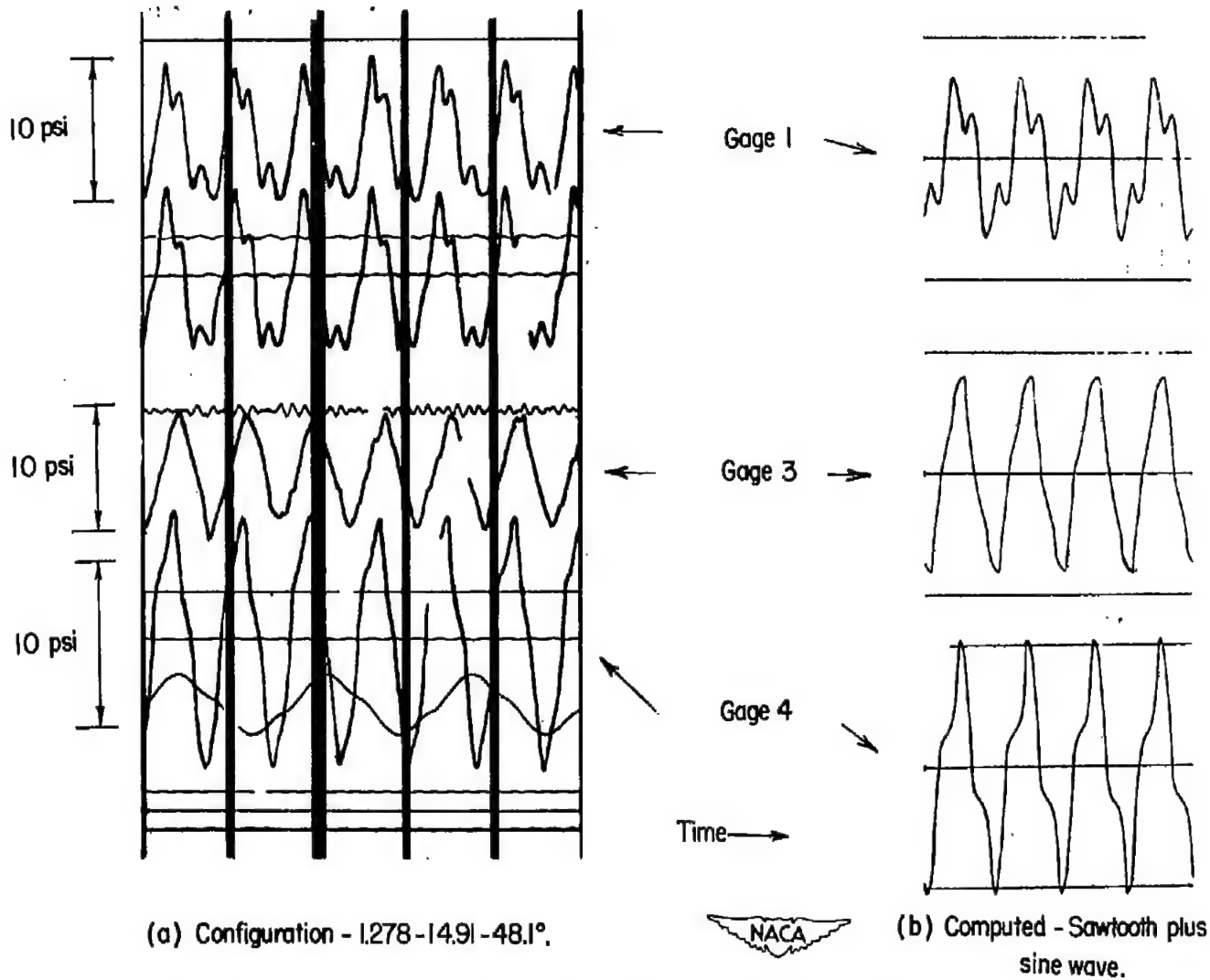

Figure 23.- Comparison of experimental pressure-time record with pressure-time record obtained by adding sine and sawtooth pulses.

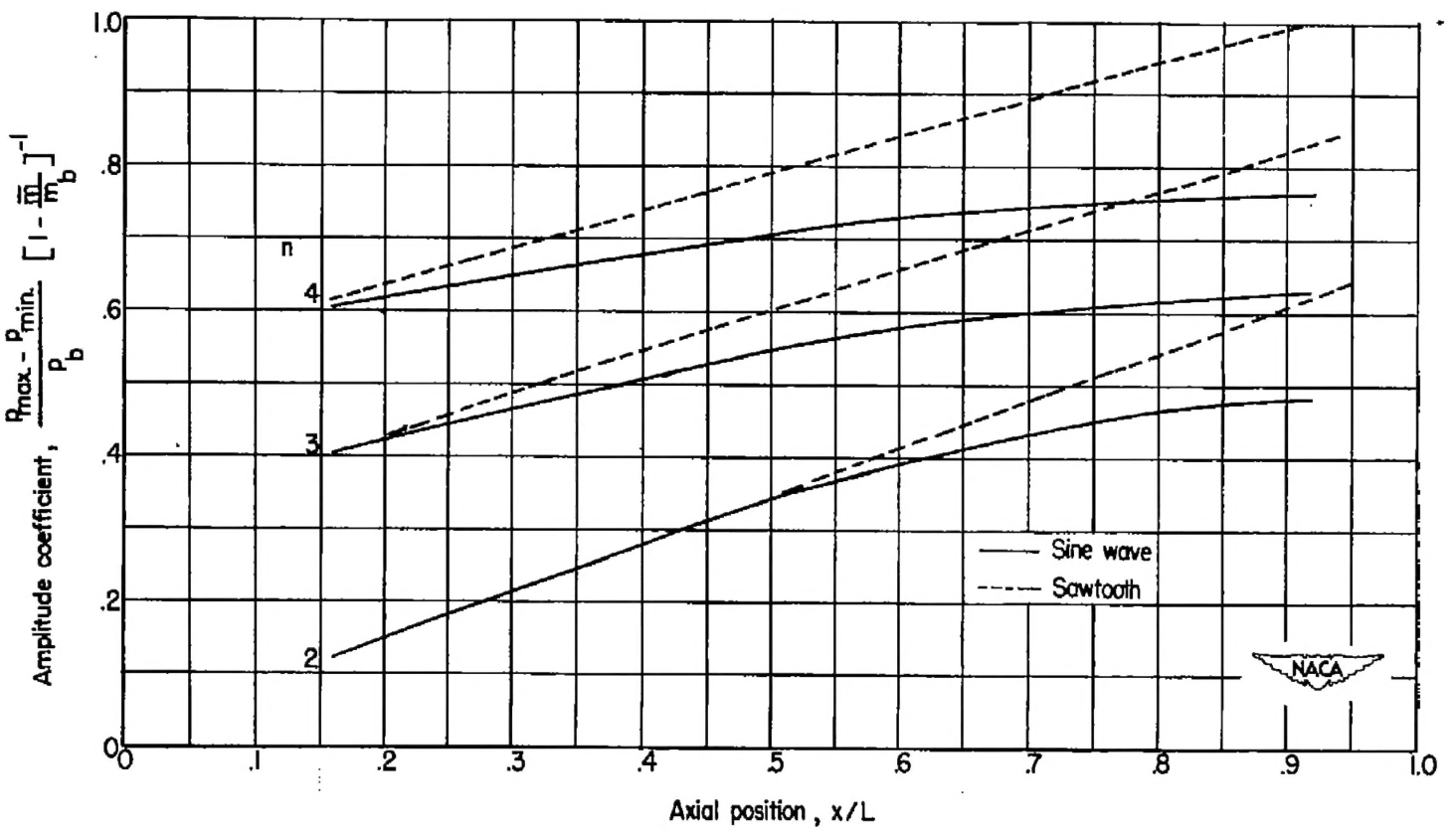

Figure 24.- Variation of pressure amplitude coefficient with axial position for $M_b = 0.14$.

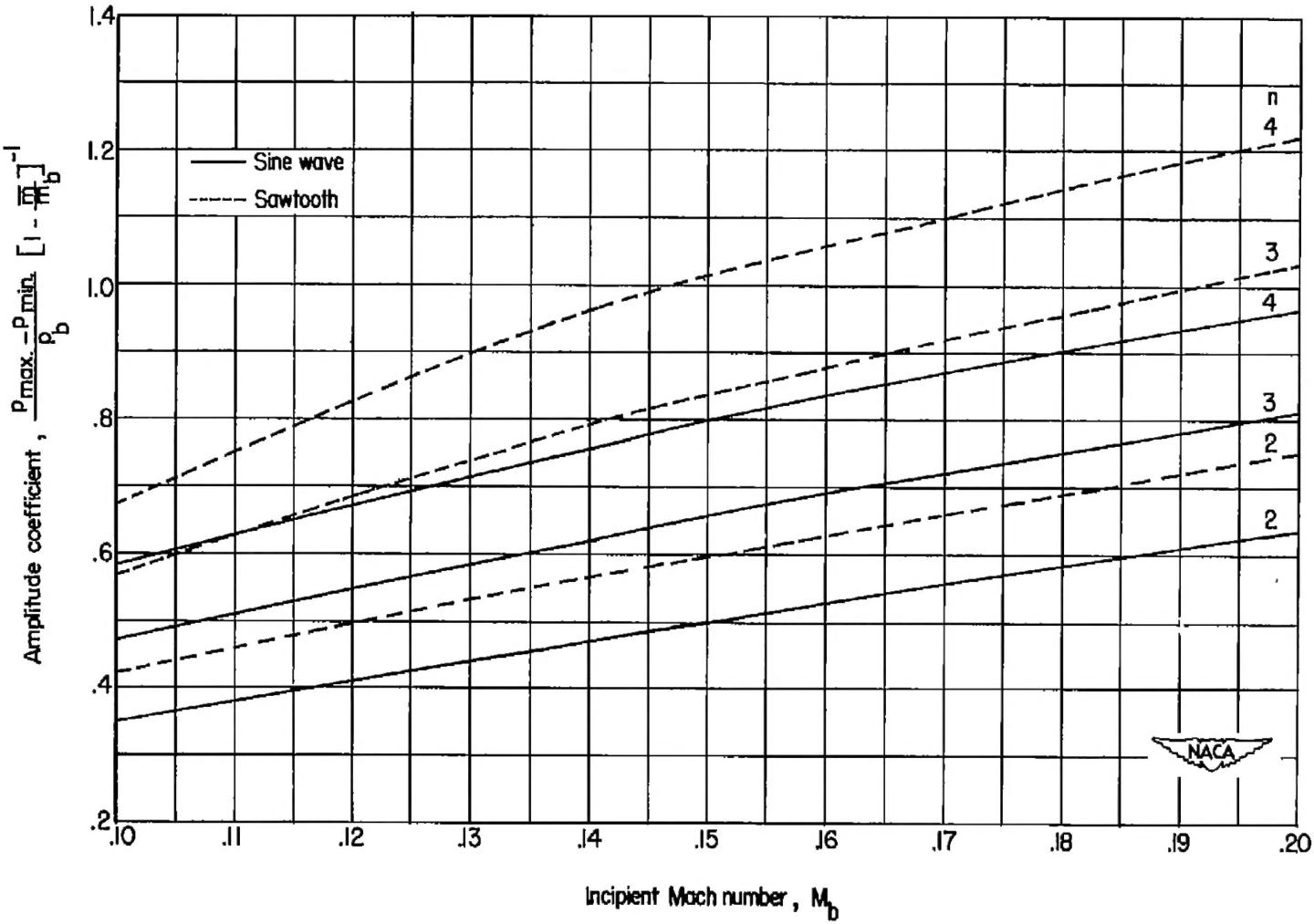

Figure 25.- Variation of pressure amplitude coefficient with Mach number at start of buzz for x/L = 0.838.

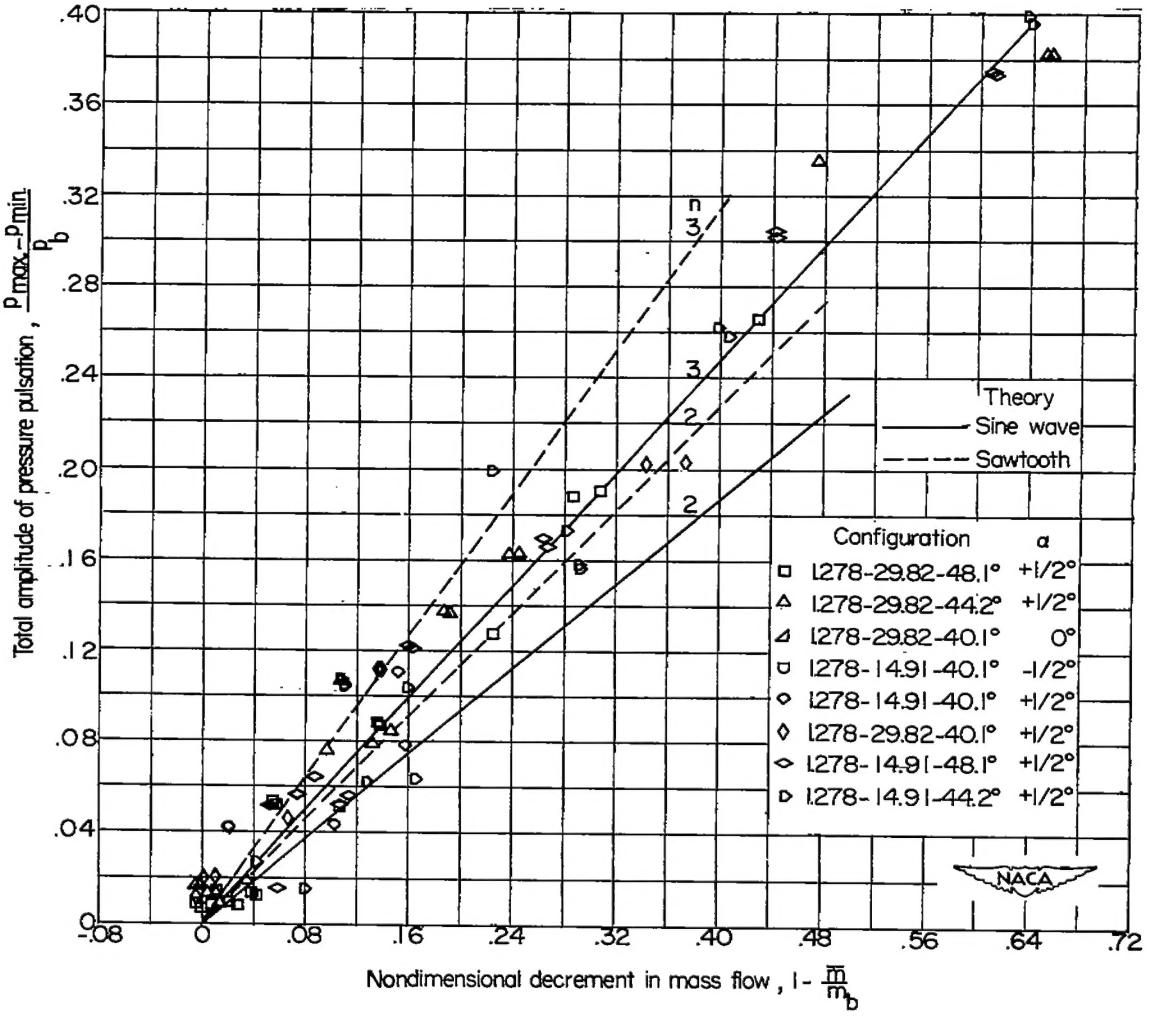

Figure 26.- Total amplitude of pressure pulsations at gage 4 plotted against nondimensional decrement in mass flow from minimum stable flow. Configurations 1.278.

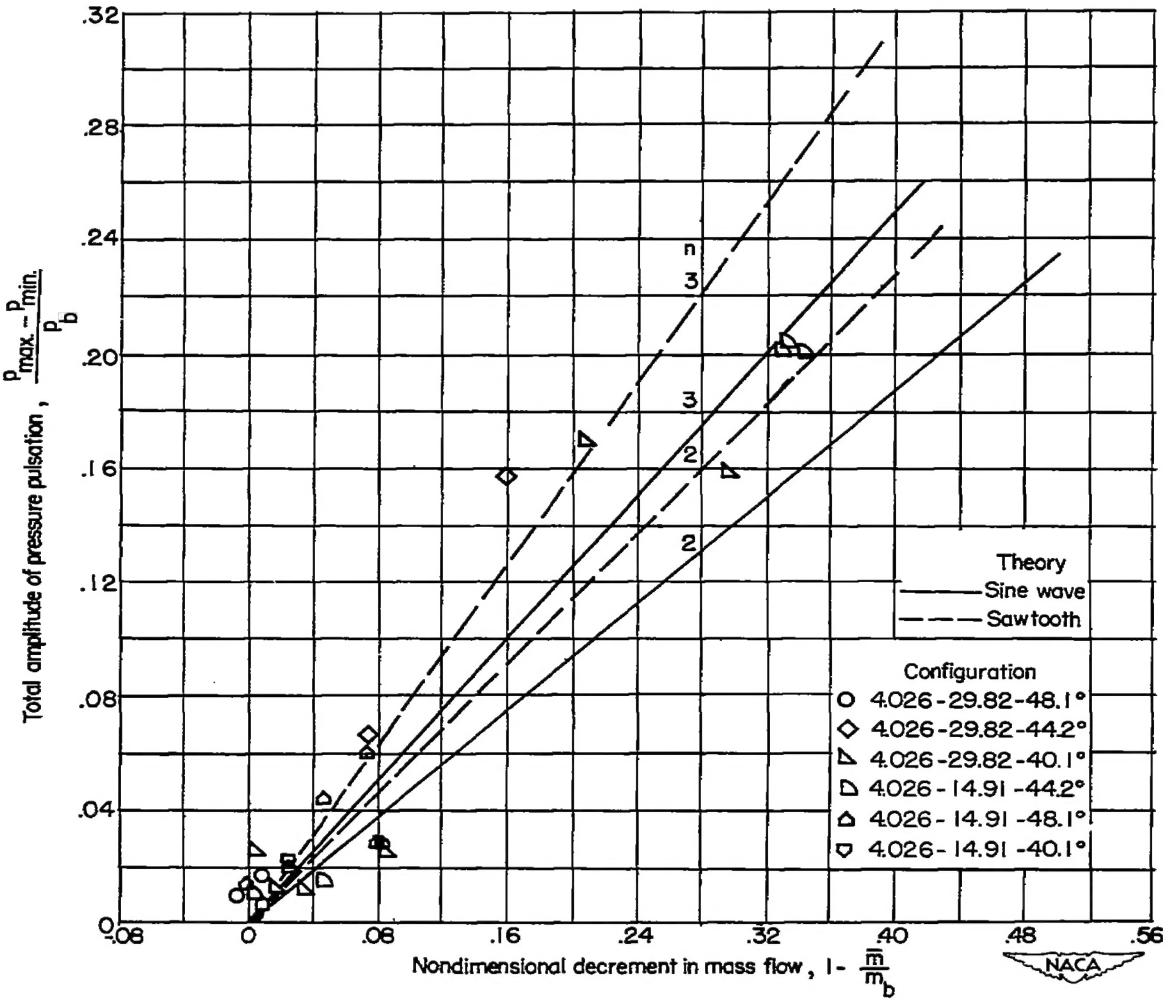

Figure 27.- Total amplitude of pressure pulsations at gage 4 plotted against nondimensional decrement in mass flow from minimum stable mass flow. Configurations 4.026; $\alpha = +\frac{1}{2}^{\circ}$.